X-651-70-419
PREPRINT

THE DEVELOPMENT OF UPWELLING ALONG THE SOMALI COAST AS DETECTED WITH THE NIMBUS 2 AND NIMBUS 3 SATELLITES

KARL-HEINZ SZEKIELDA

SEPTEMBER 1970

GSFC
GODDARD SPACE FLIGHT CENTER
GREENBELT, MARYLAND

PREPRINT

THE DEVELOPMENT OF UPWELLING ALONG THE SOMALI COAST AS DETECTED WITH THE NIMBUS 2 AND NIMBUS 3 SATELLITES

by

Karl-Heinz Szekielda

September 1970

Goddard Space Flight Center

Greenbelt, Maryland

ABSTRACT

The ground truth (validity as established by ground data) of remote-sensed equivalent blackbody temperature (T_{BB}) for the Persian Gulf as determined from Nimbus 2 satellite data was investigated. The T_{BB} values recorded with the HRIR (High Resolution Infrared Radiometer) in this region were 0.1 C° cooler than the reported ship temperatures. The standard deviation from the difference between T_{BB} values and ship measurements was 1.29, indicating that over cloud-free regions very good accuracy from orbiting sensors can be obtained. The T_{BB} recordings along the Somali Coast showed the development of upwelled water between May 23 and June 8, 1966. The T_{BB} analysis from July 3, 4, and 6 disclosed a very complicated structure near the coast, which can be explained by cyclonic and anti-cyclonic gyres. The temperature structure was confirmed by conventional ship data.

The coldest temperatures were found on July 16 at 10°N near the coast with temperatures below 15°C. A very strong thermal gradient appears during the upwelling period between the Gulf of Aden and the adjacent sea. This indicates that the gulf has a separate surface circulation.

Upwelling was remarkably reduced in September and disappeared at the end of October. Three orbits from Nimbus 3 recording T_{BB} along the Somali Coast revealed in connection with the observations aboard Nimbus 2 that the response time of upwelling to the onset of the Southwest Monsoon is less than 10 days. An estimate of the geostrophic current velocity can be obtained from the horizontal temperature gradient along the Somali Coast.

CONTENTS

THE DEVELOPMENT OF UPWELLING ALONG THE SOMALI COAST AS DETECTED WITH THE NIMBUS 2 AND NIMBUS 3 SATELLITES

by

Karl-Heinz Szekielda*

Goddard Space Flight Center

INTRODUCTION

The Nimbus 2 satellite was launched on May 15, 1966, in a near-circular orbit with an apogee height of 1180 km and a perigee height of 1095 km. During its lifetime from May to November 1966, much new information in meteorology (Warnecke, 1967), geology (Pouquet, 1968), and oceanography** (LaViolette and Seim, 1969) were telemetered. In the following study, the observations with the HRIR (High Resolution Infrared Radiometer) along the Somali Coast were used to follow the development of the cold water which is present during the Southwest Monsoon period.

The surface water masses during the Southwest Monsoon near the Somali Coast can be traced to three different origins (Warren, Stommel, and Swallow, 1966):

(1) A warm saline water from the northern edge of the Arabian Sea.

(2) A warm saline water from the Gulf of Aden.

*On leave from the Faculté des Sciences, Marseille, as a National Academy of Sciences-NRC Post Doctoral Associate.

**Warnecke G., L. J. Allison, L. M. McMillin, and K-H. Szekielda. Remote sensing of ocean currents and sea surface temperature changes derived from the Nimbus II satellite. *J. Phys. Oceanogr.* (in press).

(3) Fresher water with a salinity less than 35.3% which is transported by the South Equatorial Current from the Bay of Bengal and is brought by the Somali Current along the East African Coast to the north.

During the Southwest Monsoon, the Somali Current flows in a northerly direction as a western boundary current from below the equator. Contrary to the other western boundary currents (e.g., the Kuroshio and the Gulf Stream), the Somali Current sets at about 9°N in an eastern direction and then turns into an anticyclonic surface current at a distance of about 150 miles from the coast. Investigations with the R. V. Argo in August and September of 1964 revealed that the Somali Current is a very well defined and intense narrow stream (Stommel and Wooster, 1965). It differs only in a few points from the other currents mentioned. The most important point is that the Somali Current is present for only part of the year. Just north of the region where the current leaves the coast, strong upwelling appears; temperatures below 20°C appear between Ras Hafun and Ras Mabber. This cold water (as low as 13°C) was marked by surface fog, dead fish, and undersaturated oxygen values, as reported by Stommel and Wooster (1965). The intensity of the upwelling along the Somali Coast depends upon the geostrophic slope of the isotherms, which are a function of the strength of the current. Therefore, upwelling along the Somali Coast depends upon the wind stress and the monsoon season. Stommel and Frasetto* showed that there is very little time lag between the appearance of cold water and the onset of the Southwest Monsoon. This was judged to be true from daily minimum temperatures averaged over a month recorded at Dante (10°25′14″N, 51°15′54″E). There the wind blows over a 60-mile-wide oceanic area along the coast; therefore, low air temperatures reflect the change of SST

*Stommel H. and R. Frasetto. The time of response of the Somali Current to the Southwest Monsoon (unpublished manuscript).

(sea surface temperature). At 10°N, the Southwest Monsoon is already well developed by the last week in May. A decrease in air temperature was observed in June, and a minimum was observed in July. From these observations it can be concluded that the response time of current to wind stress should be of the order of days, and fast temperature changes can be predicted for that region.

Temperature measurements taken again near Guardafui revealed that a rapid change of SST occurs over a period of a few days, which can be explained by varying wind stress.

BACKGROUND FOR THE REMOTE SENSING OF THE OCEAN'S SEA SURFACE TEMPERATURE

The thermal behavior of a water surface can be regarded as that of a blackbody, and Planck's law is valid if the emissivity of water is considered to be 1:

$$W_\lambda = \frac{c_1 \lambda^{-5}}{[\exp(c_2/\lambda T) - 1]},$$

where c_1 and c_2 are known as the first and second radiation constants, respectively, and have the values $c_1 = 3.74 \times 10^{-12}$ W-cm^2 and $c_2 = 1.44$ cm-°C.

The thermal radiation from the earth detected with an orbiting radiometer can therefore be used for a determination of temperature at the earth's surface, if the emissivity of the area under investigation is known. This is valid only over cloud-free regions. The radiative transfer equation over a cloud-free region in an atmospheric window can be written

$$N_w = N + \frac{1}{\pi} \int_{\lambda_1}^{\lambda_2} \Phi(\lambda) \epsilon_S(\lambda) \beta(\lambda \tau_S) d\lambda ,$$

where Φ is the filter function [$\Phi(\lambda) = 0$ outside the interval $\lambda_1\lambda_2$], ϵ_S is the emissivity of the radiating surface, and $\beta(\lambda T_S)$ is the Planck function. The term N represents the energy absorbed by atmospheric gases and water vapor during the radiation from the earth's surface to satellite height. In this study, N is kept constant over the area under investigation; therefore, the reported temperatures should be regarded only as relative values, although the temperature changes in the same region are absolute.

THE RADIOMETER

A schematic representation of a radiometer that can detect outgoing radiation from the earth aboard a satellite is given in Fig. 1. The radiation emitted by the earth's surface reaches a scan mirror, which is inclined 45° to its own axis of rotation. This scanning rotates the field of view of the detector through 360° in a plane perpendicular to the orbital plane. The radiation reflected from the scan mirror is chopped at the focus, passes through a filter, and is refocused at the lead selenide detector. The output of the detector is directly proportional to the radiation received from the earth. In-flight calibration is achieved through alternate views of space and the spacecraft housing, the temperature of which is monitored during each scan.

The effective spectral response of the radiometer is defined as

$$\phi_\lambda = R_\lambda F_\lambda A_\lambda ,$$

where R_λ gives the combined spectral reflectivity of all front surface mirrors, F_λ is the spectral transmittance of the filter, and A_λ is the spectral response of the detector.

Preflight calibrations have been made in the laboratory, with the radiometer's field of view being filled with a blackbody target whose temperature could be varied. The spectral

radiance of the target with equivalent blackbody temperature (T_{BB}) is determined by the Planck function, B_λ.

The effective radiance $\bar{N}$ received at the radiometer is given in the following equation:

$$\bar{N} = \int_0^\infty B_\lambda(T_{BB})\phi_\lambda d\lambda .$$

The effective radiance $\bar{N}$ for the orbiting radiometer is the λ-integral of the spectral radiance N_λ in the direction of the satellite from the earth and its atmosphere multiplied by the spectral response ϕ_λ:

$$\bar{N} = \int_0^\infty N_\lambda \phi_\lambda d\lambda .$$

All measurements from orbit must be expressed in terms of the equivalent temperature of a blackbody (filling the field of view) that would cause the same response at the radiometer.

DATA PROCESSING

The analog signals obtained from the HRIR aboard the satellite were digitized and computer processed; calibration and the geographic coordinates were applied automatically on the digital tape. This NMRT-HRIR (Nimbus Meteorological Radiation Tape) was used to generate grid print maps. For the study along the Somali Coast, Mercator projection charts of 1:2,000,000 scale have been printed by computer; only in a few cases, where more detailed information was required, were charts in the 1:1,000,000 Mercator format used. A mathematical filter to eliminate a 200-Hz component in the noise level was developed by McMillin (1969) and applied in the following study. All data recorded from the orbiting

radiometer within a nadir angle greater than 60° were eliminated during the computer processing of the charts.

The selected orbits showed the region of study in the center of the satellite track; a nadir angle of less than 40° can be assumed for the reported results. Thus, the absorption of radiation by atmospheric gases could be assumed constant over the whole angle of view. An error less than 1 C° is produced by this assumption (Kunde, 1965). To reduce the error of geographic referencing from the computer, thermal gradients between water and land masses were used to indicate more accurate coastlines. An example is seen in Fig. 2, where the coastline from the Persian Gulf can be reproduced from the sharp thermal gradient recorded with the Nimbus HRIR radiometer. Comparison between the coastlines indicated on the working and nautical charts showed a deviation of the order of 0.5°. This small deviation was found also near the Somali Coast, where, in general, the computer-produced geographic reference error was less than 0.2°. It must be stressed that for the entire study, the orbits were preselected with the photofacsimile film strips, and orbits with a visible error in the pitch axis were already omitted.

During the fully developed upwelling at the Somali Coast, the thermal gradient between the continent and the water is not well pronounced; this is because at night along the coast the temperature of the land approaches that of the water. Therefore, the island Socotra and a mountain on the neighboring mainland, both of which emit less radiation than the surrounding area of water, were used as a reference to correct the coordinates.

Isolines were drawn in 1-C° intervals, and the resulting charts were smoothed at least over the ground resolution of the satellite recordings. Single values that appeared in the chart as single and separated isolines were disregarded, but their number never exceeded 0.2% of the total grid print points.

GROUND TRUTH OF REMOTE-SENSED SEA SURFACE TEMPERATURE FROM THE NIMBUS 2 SATELLITE IN A TEST AREA (PERSIAN GULF)

Previous methods for obtaining SST from satellites have produced different results, which may have been caused by cloud contamination, system errors, instrumental noise, and theoretical corrections for water vapor and absorption by atmospheric gases; therefore, this study makes no attempt to derive "true" SST's. Instead, T_{BB}'s measured by the same satellite radiometer over cloud-free regions should reveal highly significant relative changes and gradients in SST.

The Persian Gulf has been chosen as a test area over which to investigate the ground truth (validity as established by ground data) for the two following studies:

(1) The seasonal fluctuation of temperatures recorded by a satellite in a given region.

(2) The relative accuracy of the recorded T_{BB} values aboard the satellite.

The second study has been made with reported ship temperatures in the Persian Gulf. Because the results present the first systematic handling of satellite data for oceanographic purposes, they are published also in this paper; thus, the reader can form his own views of the temperature structure along the Somali Coast.

Hydrographic Features in the Persian Gulf

The Persian Gulf resembles a Mediterranean Sea with an arid climate; that is, evaporation exceeds precipitation, and water is formed with a high salinity. This increase in salinity takes place during the transport of surface water from the Gulf of Oman through the Strait of Hormuz to the northern edge of the Persian Gulf, as a result of the excess of evaporation over precipitation. Consequently, water with density as high as $\sigma_t = 26$ can build up at the surface and will sink to the bottom. This dense, warm, and saline water will then be transported over the bottom into the neighboring Arabian Sea.

The buildup of highly saline water is not limited to the summer months; it is a continuous process and depends on winds and temperature. The supply of river water from the Euphrates and Tigris is limited to a small region of the gulf and can be traced by low salinities, lower temperatures, and lower densities southward along the Arabian Coast. A freshening of the northern gulf water by the greatest runoff from the Euphrates and Tigris occurs during spring and early summer: this results from snow melting in the Armenian mountains.

A yearly fluctuation in temperature is evident: a mean temperature of 15°C was observed during February in the northwest corner of the Persian Gulf; the maximum reported up to now is 36°C for the southern Persian Gulf, as shown in Table 1.

At the end of the Southwest Monsoon, a heating of the upper water layer is introduced, and temperature values up to 33°C were observed by Emery (1956); also, 36.5°C has been reported by Blegvad (1944) near the Bahrein Islands. The high change of temperatures from about 36°C in summer to about 15°C in February was reported at Bandare Shahpur.

Seasonal Temperature Changes Observed With the HRIR

For the purpose of this Nimbus 2 HRIR study, all available cloud-free nighttime orbits over the Persian Gulf recorded from June through September 1966 were analyzed from computer-produced grid print maps.

Mean T_{BB} values were calculated for the Persian Gulf from approximately 350 scan spots that covered individual areas 9 to 12 km in diameter for the northern and southern regions. The regions covered are shown by the two squares in Fig. 2.

Historical SST's for these two regions indicated a seasonal SST range of 15 C° and a 1.7 C° regional temperature difference between the southern and northern areas. This

Table 1—Mean temperatures (°C) in the Persian Gulf, after Schott (1908).

Month	Location (East Longitude)						
	48°-49°	49°-50°	50°-51°	51°-52°	52°-53°	53°-54°	54°-55°
December	18.4	20.3	21.6	22.6	23.3	23.5	24.2
January	16.0	17.3	19.7	20.8	21.1	21.4	22.1
February	15.2	16.4	18.1	19.4	19.8	20.9	21.8
March	17.0	17.7	19.1	20.0	20.8	21.8	22.0
April	19.8	20.7	22.0	22.6	23.2	23.8	24.1
May	24.5	25.0	25.5	26.0	26.3	26.9	27.0
June	27.4	27.8	28.4	28.2	28.4	28.6	28.9
July	29.6	29.8	30.4	30.4	31.2	31.0	31.0
August	31.9	31.5	31.2	31.8	32.0	32.4	32.3
September	29.8	30.0	31.1	31.7	31.8	31.9	31.8
October	27.5	28.7	29.4	29.6	29.9	30.3	30.5
November	22.8	24.1	25.6	26.1	27.3	27.6	27.9
Number of observations	86	243	595	326	260	241	242
Yearly average	23.3	24.2	25.2	25.8	26.2	26.7	27.0
Absolute maximum	33.1	33.1	34.5	34.2	34.5	36.0	34.9
Date	August 11	August 21	August 5	August 17	August 17	August 17	August 21
Absolute minimum	13.8	12.3	15.8	16.3	18.0	17.9	17.9
Date	February 20	January 22	February 20	February 20	March 10	February 12	January 17

regional difference, if apparent in the satellite radiation data, proves the validity of these measurements. The variations of mean blackbody temperature values in centigrade degrees for the Persian Gulf from June through November 1966 are shown in Fig. 3. The solid curve represents the temperature changes in the southern portion; the dashed curve corresponds to temperature changes in the northern part. Two pronounced maxima are apparent in both curves: one in mid-June and the other in mid-September 1966.

In mid-June, extremely high SST's (49°C by day and 46°C at night) were recorded by weather stations in the area. In general, the Persian Gulf SST changes follow the changes in surface air temperature; high SST's could be expected from high air temperatures alone.

The second T_{BB} maximum occurred in mid-September at the end of the Southwest Monsoon. This is a period when wind-induced vertical mixing is reduced and surface water is warmed appreciably. With the onset of the Northeast Monsoon in October, a sharp decrease in sea temperature was observed in the satellite data. A mean difference of 1.3 C° was noted between averaged nighttime HRIR data over the warmer southern portions of the gulf and corresponding data over the cooler northern portions; this agrees with historical SST data of 1.7 C° mean difference.

Normally, we find lower temperatures in the northern part of the gulf. Mean values from all reported salinities in Table 2 indicate that the highest runoff from the Euphrates and Tigris occurs in June. Since the influence of the outflowing water is limited to the coast, colder water in the northern part of the gulf can be explained by transport of cooler water from deeper horizons to the surface or by cooling through evaporation. Winds are found to predominate between west and northwest during the year. Because of displacement of surface water by these winds, intense vertical mixing can be expected in the northern part of the gulf; this gives an explanation for the cooler water.

Table 2—Mean salinities in the Persian Gulf as averaged from data reported by Dubach (1964).

Month	Location (East Longitude)						
	48°-49°	49°-50°	50°-51°	51°-52°	52°-53°	53°-54°	54°-56°
May	–	39.92	39.73	38.85	38.85	–	37.97
June	26.09	39.93	–	38.94	37.75	37.84	37.46
July	–	–	–	–	–	–	–
August	–	–	39.39	39.50	38.68	39.54	38.79
September	–	–	–	–	–	–	–
October	–	40.27	39.67	39.44	38.00	39.54	38.12
November	40.70	40.26	40.01	–	–	–	–
December	40.06	–	40.02	–	–	–	–

A detailed temperature analysis from a computer-produced, 1:1,000,000 grid print map for the northern part of the gulf on June 14 showed water cooler than 31°C. The lowest temperatures are found in the north near the coast and indicate that the surface layer is driven away from the coast and replaced by layers from below.

An analysis from the few ship observations of currents establishes that two separated cyclonic eddies exist in the Persian Gulf; this explains the persistent difference in temperature between the northern and southern regions.

An example of the persistence of cold water in the northern Persian Gulf (observed from orbit on June 26) is shown in Fig. 4. Cold water can be recognized by the position of the 29°C isotherm and the well-developed gradient.

Figure 5 shows T_{BB} distribution in the gulf during the second warming period, as observed from four nighttime orbits in September. The shaded areas show the persistence of warmer water masses with T_{BB} values above 34°C in the shallow southern region.

This qualitative study has shown that seasonal temperature changes, short-term anomalies, and patchiness in sea surface temperatures can be detected by the use of satellite data if careful choice of orbit is made to avoid cloud contamination over the area of study.

Statistical Comparison Between Ship Observations and Satellite SST Measurements

The statistical treatment of the difference between T_{BB} values and temperatures reported from ships is based on 27 observations. The T_{BB} resulting from a 1:2,000,000 grid print map were compared with reports from ships, whose positions were determined within the corrected grid print map position as described above. The results are given in Table 3.

The mean value showed that the satellite radiation temperature was 0.1 C° below that indicated by ship data. The calculated standard deviation

$$\sigma = \sqrt{\frac{\sum_{i=1}^{n} x_i^2 - \bar{x}^2}{2}}$$

for the difference between ship data and T_{BB} values was 1.3 C°.

The diurnal cycle of the surface temperatures in the Persian Gulf is included in the above calculation, because only in a few cases were temperature measurements aboard ships made during satellite overpass. Also, errors in ship measurements must be taken into account.

A comparison between actual T_{BB} values and ship observations is seen in Fig. 6, where six ship temperature values were available over 24 hours and are included in the grid print HRIR map for September 27.

Table 3—Comparison of sea surface temperatures observed by ships and Nimbus 2 in the Persian Gulf during 1966.

Date	GCT	Latitude (°N)	Longitude (°E)	Clouds	t (°C)	Δt (air – sea, in C°)	T_{BB} (°C)	Δt ($T_{BB} - t$, in C°)	Ship
June 3	12/18	24.5	58.5	0	32(2)	−1	31	−1	Kenai Peninsula
June 8	12/18	24.5	59.0	0	29(2)	+3	33	+4	Torrey Canyon
June 13	00/06	24.5	58.0	0	32(2)	±0	33	+1	Mobil Brilliant
June 16	06	27.0	53.0	0	29	+2	30	+1	Esso Chile
	12	26.0	54.0	0	32	−1	31	−1	
	18	26.0	56.0	0	32	−2	31	−1	
June 17	00	26.0	57.0	0	32	−1	33	+1	Esso Chile
	06	25.0	58.0	3	32	−1	33	+1	
	12			0	32	+1	31	−1	
July 5	06	26.0	54.0	0	32	±0	31	−1	Northfield
September 4	00	28.0	51.0	0	34	−2	32	−2	Petroqueen
	06	27.0	52.0	0	34	±0	34	±0	
	12	26.0	54.0	0	35	−2	33	−2	
September 17	12	26.0	55.0	0	33	+1	32	−1	Petroqueen
	18	26.5	53.0	0	34	−2	32	−2	
September 23	06	29.0	50.5	0	33	±0	33	±0	Trautenfels

Table 3–Continued.

Date	GCT	Latitude (°N)	Longitude (°E)	Clouds	t (°C)	Δt (air – sea, in C°)	T_{BB} (°C)	Δt ($T_{BB} - t$, in C°)	Ship
September 27	00	28.5	50.0	0	33	−2	32	−1	Trautenfels
	06	27.5	51.5	0	32	−4	33	+1	(see Fig. 8)
	12	26.5	53.0	0	33	−1	33	±0	
	18	26.5	54.5	0	32	−1	33	+1	
September 28	00	26.5	56.0	1	30	−1	30	±0	
	12	25.0	59.5	1	30	−1	30	±0	
October 3	18	24.5	58.0	8*	29	±0	28	−1	Wabasha
October 3	12	24.5	58.0	0	30	+6	31	+1	Petersen
	18	26.0	57.0	0	30	−1	30	±0	
October 4	00	26.5	55.5	0	32	−2	31	−1	Petersen
	06	27.0	54.0	0	33	+1	33	±0	

*Uncertain.

RESULTS OF THE DETECTED UPWELLED WATER ALONG THE SOMALI COAST

Representation of the T_{BB} Distribution Charts

The typical temperature distribution for a part of the Arabian Sea during the Southwest Monsoon can be discussed on the basis of a temperature chart obtained with Nimbus 2 on September 9, where cloudfree areas appeared between the equator and 10°N. The recorded infrared data interpretated in terms of T_{BB}'s were averaged over 1 square degree of area and are shown in Fig. 7.

Along the Somali Coast, upwelling is characterized by temperatures below 23°C. The Southwest Monsoon drift, which represents an anticyclonic water movement at the surface, is recognizable by temperatures higher than 27°C in the inner part of the anticyclonic movement. The highest temperatures were 29°C at about 63°E and 3°N.

The temperature charts from the Somali Coast are presented in chronological order, starting with the T_{BB} distribution on May 23, 1966 (Fig. 8). At this time the distribution of temperatures showed no special features, and only the decrease in temperature from the Arabian Sea to the Gulf of Aden is remarkable. On June 8 (Fig. 9), the upwelling at Ras Hafun was starting; this can be recognized by temperatures below 23°C near the coast and the building of a thermal gradient parallel to the coast. The highest temperatures (30°C) were observed east of the upwelling region. The orbit on June 10 shows (Fig. 10) similar temperature patterns. The principal differences are the increase of area with temperatures below 23°C and the temperature difference between the Gulf of Aden and the adjacent sea. The 22°C isoline indicates that different cores of upwelling water occurred along the coast. These cores are still visible with the next available orbits in July, when temperatures were

below 22°C. Strong thermal gradients similar to the recordings from June 8 were observed. A very strong gradient between the water from the Gulf of Aden and the adjacent sea was built during the upwelling period along the Somali Coast. Its development was recorded from satellite data. The first indication of its presence was given in the T_{BB} recordings of July 2 (Fig. 11), where the temperature difference between the Gulf of Aden and the adjacent sea was about 4 C°.

Infrared recordings with Nimbus 2 on July 3 covered a large region near the Somali Coast and the neighboring sea (Fig. 12). This analysis allows one to conclude that an anticyclonic water movement exists along the Somali Coast, accumulating warm water in the inner part of the gyre, with temperatures higher than 26°C.

An anticyclonic water movement near the Somali Coast was first described by Findlay (1866) and was investigated more recently by Bruce (1968) and Düing.* In Findlay's chart, an anticyclonic gyre is also reported for the Gulf of Aden and thereby helps to confirm the existence of the anticyclonic motion inferred from the distribution of SST observed from Nimbus 2 in the same area. Northeast off Socotra, temperatures below 24°C were observed; these are probably in the center of a cyclonic water movement. An isolated warm area at 56°E and 11°N suggests another anticyclonic water movement.

The diameter of the detected whirls ranges between 100 and 300 miles; however, a photograph taken aboard a manned spacecraft showed that, in this region, eddies with smaller diameters can appear. The temperature gradient at the eastern edge of the Gulf of Aden is always present during the fully developed upwelling along the Somali Coast. Its strength has not necessarily coincided with the strength of the movement in the inner part

*Düing W. (1970) The monsoon regime of the currents in the Indian Ocean (in press).

of the gulf because the temperature effect on density can be somewhat compensated for by a different salinity.

The recorded temperature on July 4 shows a distribution pattern similar to that recorded on July 3 along the Somali Coast, but a stronger cooling than before was observed over the entire area (Fig. 13). In the southern core of the upwelling, a temperature decrease of 2 C° over a small area appeared; greater regions showed a decrease of only 1 C°.

For a comparison with the temperature patchiness as recorded by the satellite HRIR, only a few ship measurements were available. Table 4 gives SST observations made aboard the SS Wabasha during July 7-9, 1966. These measurements largely confirmed the results from the Nimbus 2 HRIR. The SS Wabasha crossed the cyclonic gyre near 13°24′N, as can be seen from temperatures below 25°C, with higher temperatures before and after it crossed the gyre. At 9°48′N, 54°24′E, the transportation of cold water away from the coast is evident from the ship measurements (22.2°C), south of which an SST increase to 27.8°C was observed. Far to the south, temperatures were below 26°C.

Although the satellite and ship data were not obtained at the same time, they showed the same SST patchiness. Chlorophyll measurements during the Southwest Monsoon showed a similar patchiness, which may be explained by the presence of separated cyclonic and anticyclonic rate movements over the entire Arabian Sea. Figure 14 presents the integrated chlorophyll concentrations from the surface to 200 m along 10°N. The samples where maxima appear near the coast have been collected during one 24-hour period (August 29-30); therefore, their relative positions are significant.

The chlorophyll maxima need a detailed discussion because they can be produced by divergent water movement or by transport of nutrient-rich water from the upwelling to the inner part of an anticyclonic water movement (Szekielda, 1969). Consequently, the time

Table 4– Sea surface temperatures observed aboard the SS Wabasha along the Somali Coast in 1966.

Date	Position		SST (°C)
	Latitude (degrees)	Longitude (degrees)	
July 7	14.6	56.5	27.8
July 8	13.4	55.9	24.4
	12.2	55.5	26.7
	11.0	54.9	25.6
	9.8	54.4	22.2
July 9	8.6	53.8	26.1
	7.2	53.5	26.7
	5.9	53.0	27.8
	4.7	52.3	25.6

lag between the transport of nutrients to the surface and their influence on biological processes must be considered.

On July 6, the anticyclonic movement near the coast was excellently visible, along with the T_{BB} distribution (Fig. 15). The ship observations of July 9 in Table 4 indicated a temperature patchiness similar to that observed on July 3 and 4 from the satellite. The different temperatures on July 6 must be explained by different meteorological conditions. The analyzed wind observations near Socotra showed that wind speeds in that region are not constant. Therefore, vertical mixing resulting in different SST's can be expected over a short time interval in that region.

The sequence of observations from July 2 to July 6 suggests that cold water patches generated by upwelling in the neighborhood of Ras Hafun are advected along the outer edge of the anticyclonic eddy. On July 2, an attempt to trace an isolated patch of cold water with temperatures below 20°C was made. It may have travelled approximately 240 miles

between July 2 and July 4, corresponding to an average speed of 5 knots. It may have travelled approximately 120 miles between July 4 and July 6, corresponding to an average speed of 2.5 knots. These values compare favorably with the current measurements made off the Somali coast by Swallow and Bruce (1966) during the Southwest Monsoon period of 1964. The mechanism of the building of the cold patches can be explained by variations in wind stress, tidal currents, and internal waves in the coastal area.

The transportation of cold water away from the coast, as indicated by T_{BB} distribution, is confirmed by conventional current measurements. According to Bruce* (1968), observations during the Southwest Monsoon showed that the highest velocities appear within a very narrow boundary near the coast. Current speed increases from south to north to that region where the current turns to the east. High velocities appear, with maxima to about 300 cm-sec^{-1} in the north. Only north off Ras Hafun was low current speed observed along the coast, but between Socotra and Guardafui some measurements still showed northward flow of the upwelled water.

The lowest temperatures along the Somali Coast were measured from Nimbus 2 on July 15, when temperatures below 15°C near Ras Hafun appeared (Fig. 16). At that time, only one core of cold water was detected. This shows that the two cores of upwelled water shown in Figures 10, 11, 12, 13, and 15 are a local effect during the development of the cold water. In agreement with the low temperatures near the coast, the horizontal temperature gradient reached its maximum during July. On August 13 (Fig. 17), the intensity of

*Bruce J. G. (1965) Near surface currents off the Somali Coast in the summer monsoon, August 1964. Woods Hole Oceanogr. Inst. Tech. Report (unpublished manuscript); and Bruce J. G. (1966) Near surface currents off the Somali Coast in the summer monsoon, August 1964, Part II. Woods Hole Oceanogr. Inst. Tech. Report (unpublished manuscript).

upwelling was slightly reduced, although the surface area with temperatures below 23°C was increased.

Observations from orbits on August 13 and 16 showed (Fig. 18) that offshore transportation at the surface is reduced and that the greatest temperature gradients are limited to the region near the coast and the water between the Gulf of Aden and the adjacent sea. No ship data were available for August 13 and 16, but one ship crossed the upwelling area during August 21 and 22 (Table 5).

Although the center of the upwelling water was not crossed, temperatures up to 23°C were recorded at 10°54′N, 52°42′E. The temperature change of 6 C° between 12°0′N, 49°24′E marked the sharp temperature gradient at the exit of the Gulf of Aden.

An unusual temperature gradient, which was never reported before for that region, was found at the eastern border of the Gulf of Aden on September 4 (Fig. 19). Ship observations confirmed the presence and the strength of this gradient and its variation with time and latitude. Observations from three ships that crossed the Gulf of Aden are shown in Fig.

Table 5—Sea surface temperatures observed aboard the SS Steel Fabrication during August 21 and 22, 1966.

Date	Position		SST (°C)
	Latitude (degrees)	Longitude (degrees)	
August 21	8.9	54.2	26.1
	9.6	53.3	25.6
	9.7	52.7	24.4
	10.9	52.1	23.3
August 22	12.0	49.4	29.4
	11.9	47.9	31.1
	11.8	46.3	30.6

20. The greatest temperature change was reported by the Forsvik during September 20 and 21, when it crossed the gulf off its southern coast. The President Jackson crossed the gulf a few weeks earlier off the northern edge and reported only a small temperature gradient, although a temperature decrease of 5 C° over 360 miles was observed from west to east. On the other hand, the Universe Defiance had recorded a sharp temperature gradient at 13°N. These results coincide with satellite measurements; however, the sharpest gradient lies near the African continent.

An analysis of an orbit on September 9 (Fig. 21) revealed that upwelling decreased and that only a small area had temperatures lower than 23°C.

At the end of the Southwest Monsoon, no strong thermal gradients were observed (Fig. 22), and small patterns with different temperatures had formed. It is possible that during the transition period the greater gyres broke down into smaller gyres, producing the temperature patchiness shown in Fig. 22. One photograph taken during the Apollo 7 mission shows a cyclonic eddy that separated during October between Socotra and the Somali Coast. Figure 23 is a negative print from the original color picture; it shows the presence of a whirl with a diameter of about 50 kilometers.

The Geostrophic Flow of The Somali Current

Warsh and others* related the surface temperature of the Gulf of Mexico to its circulation. The vertical gradient of the geostrophic current outside equatorial regions was written

*Warsh K. L., E. Z. Stakhiv, and M. Garstang (1970) On the relation between the surface temperature of the Gulf of Mexico and its circulation (in press).

$$\frac{\partial v}{\partial z} = -k\frac{\partial \rho}{\partial x},$$

$$\frac{\partial u}{\partial z} = k\frac{\partial \rho}{\partial y}, \tag{1}$$

and

$$k = \frac{g}{\rho f},$$

where x, y, and z are, respectively, the east, north, and up directions, u and v are the corresponding horizontal velocities, k includes the acceleration of gravity g, the Coriolis factor f, and the water density ρ. The integrated form of this equation over depth R is

$$v - v_R = \int_i^R k\frac{\partial \rho}{\partial x}\,dz$$

and (2)

$$u - u_R = -\int_i^R k\frac{\partial \rho}{\partial y}\,dz \ .$$

Density changes of the surface water in the upwelling region are produced primarily by the temperature, because salinity is almost constant over the entire area of upwelling. This means that the horizontal temperature gradient gives an indication about geostrophic velocities.

The following relationship between the current velocities and the surface temperature gradient was derived from ship measurements:

$$v_g = 3.5 \times 10^3 \frac{\Delta T}{\Delta L}, \tag{3}$$

where v_g is in centimeters per second and $\Delta T/\Delta L$ is in degrees centigrade per kilometer. The equation should also give an estimate of the geostrophic velocity near the Somali Coast. The temperature gradient at 9°N along the Somali Coast (see Table 6 and Fig. 24) revealed

Table 6--Temperature gradient at the eastern edge of the Somali Current at 9°N in 1966 as obtained from Nimbus 2 HRIR data.

Date	Gradient ($C°\text{-}km^{-1}$)
May 23	—
June 8	0.054
June 10	0.054
July 2	0.045
July 3	0.058
July 4	0.074
July 6	0.125
July 16	0.135
August 13	0.104
August 16	0.108
September 4	0.108
September 11	0.058
October 30	0.025

[as shown by equation (3)] that current velocities of the order of 300 $cm\text{-}sec^{-1}$ may appear. This agrees with current measurements reported by Bruce.* Therefore, the order of magnitude for current velocities can be derived from remote-sensed SST.

The Response Time of the Upwelling to the Southwest Monsoon

The investigations with Nimbus 2 in 1966 with regard to the thermal structure along the Somali Coast revealed that the response time to the onset of the Southwest Monsoon can be less than 14 days. The temperature gradient at the eastern edge of the Somali Current at 9°N (Table 6) indicated that upwelling was already under way by June 8. The

*Bruce J. G. (1966) Near surface currents off the Somali Coast in the summer monsoon, August 1964, Part II. Woods Hole Oceanogr. Inst. Tech. Report (unpublished manuscript).

Southwest Monsoon started at the end of May 1966; therefore a response time of about 10 days or less is indicated.

From Nimbus 3, which carried a radiometer similar to that on Nimbus 2, three orbits were available over a short period in the beginning of the upwelling along the Somali Coast. A temperature map for May 14, 1969 (Fig. 25), shows temperatures similar to those recorded in October 1966 by Nimbus 2. These months are transition periods when changes from the Northeast to the Southwest Monsoon and vice versa occur, respectively. These transition periods should show similar temperature distribution patterns but with different absolute temperatures.

The temperatures obtained with Nimbus 3 for May 14, 1969, showed high values for the entire region. Only one small area at about 8°N indicated the beginning of upwelling, but temperatures were not below 25°C. Fourteen days later, the temperatures were below 20°C, and the temperature distribution showed no pronounced gradients along the coast. On May 31, 1969, a sharp temperature gradient was recognizable parallel to the coast (Fig. 26). From the measurements with Nimbus 2 and Nimbus 3, it can be concluded that this special temperature distribution appears only over a very short period. Temperatures below 19°C were observed at two places on May 31. This shows that the different cores of upwelling are a typical feature at the beginning of the upwelling and that the general temperature patterns are similar each year.

The time from the onset of the Southwest Monsoon to the upwelling and to the increase in current along the Somali Coast can be as little as 10 days. This is the order of magnitude predicted by Cox (1970) from a model of the Indian Ocean.

ACKNOWLEDGMENTS

The author wishes to thank Dr. W. Nordberg, chief of the Laboratory of Earth and Meteorological Sciences, and W. R. Bandeen, assistant chief, for the use of the excellent working facilities in their laboratory. Miss J. E. Regala gave important help in computer processing the HRIR data. Also, L. J. Allison and P. E. LaViolette provided considerable help through their experiences in space oceanography.

REFERENCES

Blegvad H. (1944) Fishes of the Iranian Gulf. In: Danish scientific investigations in Iran. Murksgaard. Pt. III, 1-247, 1944.

Bruce J. G. (1968) Comparison of near surface dynamic topography during the two monsoons in the Western Indian Ocean. *Deep-Sea Res.* 15, 665-677.

Cox M. D. (1970) A mathematical model of the Indian Ocean. *Deep-Sea Res.* 17, 47-75.

Dubach H. V. (1964) A summary of temperature-salinity characteristics of the Persian Gulf. National Oceanogr. Data Center General Series. Publication G-4.

Emery K. O. (1956) Sediments and water of the Persian Gulf. *Bull. Am. Ass. Petrol. Geol.* 40(10), 2354-2383.

Findlay A. G. (1866) A directory for the navigation of the Indian Ocean. Richard Holmes Laurie, 1062 pp.

Kunde V. (1965) Theoretical relationship between equivalent blackbody temperatures and surface temperatures measured by the Nimbus high resolution infrared radiometer. In: Observations from the Nimbus I Meteorological Satellite NASA SP-89, 23-36.

Laird J., B. B. Breivogel, and C. S. Yentsch (1964) The distribution of chlorophyll in the Western Indian Ocean during the Southwest Monsoon period July 30-November 12, 1963. Woods Hole Oceanogr. Inst. Tech. Report No. 64-33, 1964.

LaViolette P. E. and S. E. Seim (1969) Satellites capable of oceanographic data acquisition–a review. Tech. Report TR-215 U. S. Naval Oceanographic Office, Washington, D. C. 20390, 81 pp.

McMillin L. M. (1969) A procedure to eliminate periodic noise found in Nimbus II high resolution infrared radiometer measurements. NASA Contractor Report 9 G45-32, 16 pp.

Pouquet J. (1968) An approach to the remote detection of earth resources in sub-arid lands. NASA TN D-4647.

Schott G. (1908) Der Salzgehalt des Persischen Golfes und der angrenzenden Gewässer. *Annalen der Hydrograph. und Maritimen Meteorolog.* 36, 296-299.

Stommel H. and W. Wooster (1965) Reconnaissance of the Somali Current during the Southwest Monsoon. *Proc. Nat. Acad. Sci. USA* 54, 8-13.

Swallow J. C. and J. G. Bruce (1966) Current measurements off the Somali Coast during the Southwest Monsoon of 1964. *Deep-Sea Res.* 13, 861-888.

Szekielda K-H. (1969) The effect of cyclonic and anticyclonic water movements on the distribution of organic matter. NASA TMX-63849.

Warnecke G. (1967) The remote sensing of stratospheric temperatures and some results from the Nimbus II satellite experiment. NASA TMX-55958.

Warren B., H. Stommel, and J. C. Swallow (1966) Water masses and patterns of flow in the Somali basin during the Southwest Monsoon of 1964. *Deep-Sea Res.* 13, 825-1966.

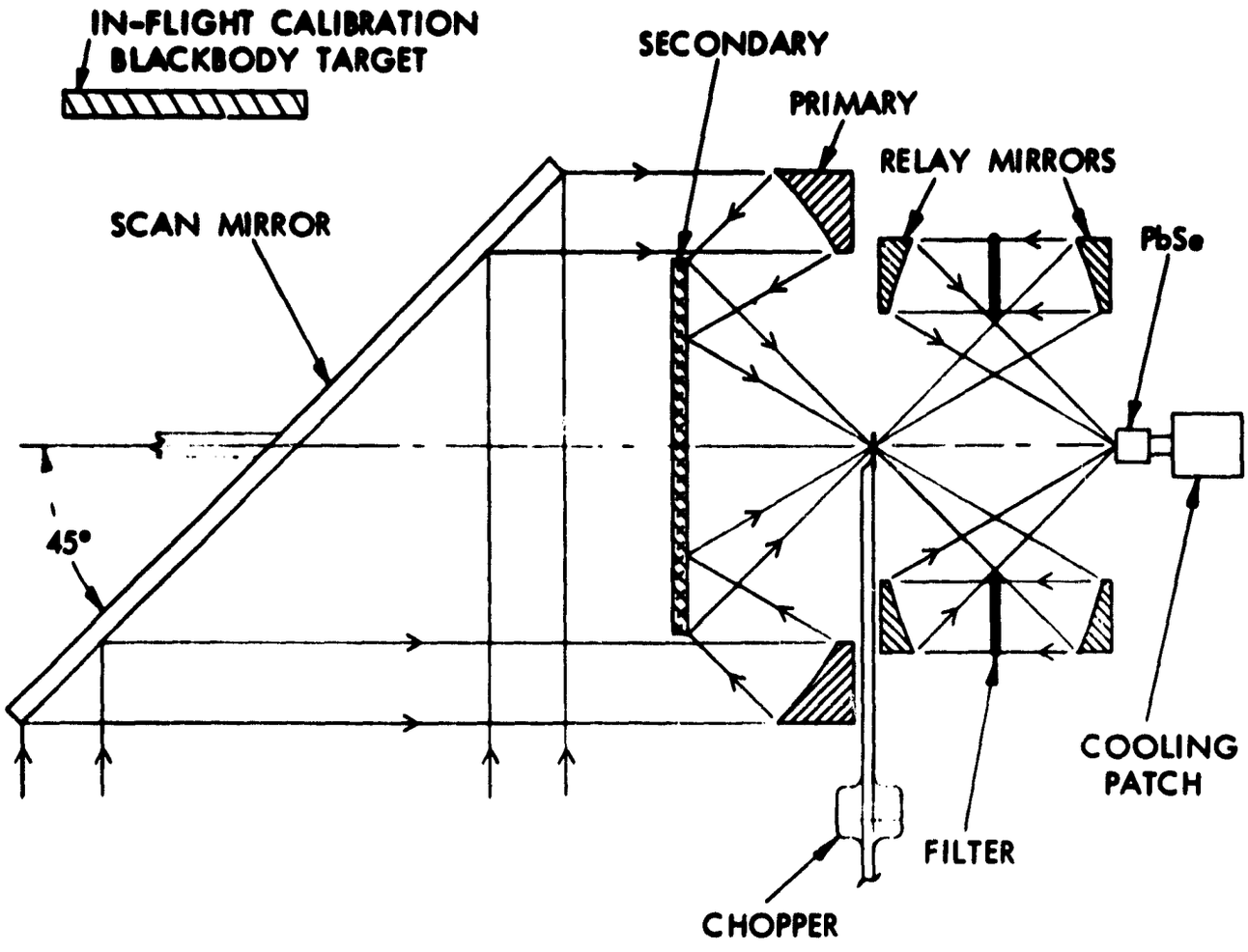

Fig. 1. The principle of the measurements to detect earth radiation aboard Nimbus 2 and Nimbus 3.

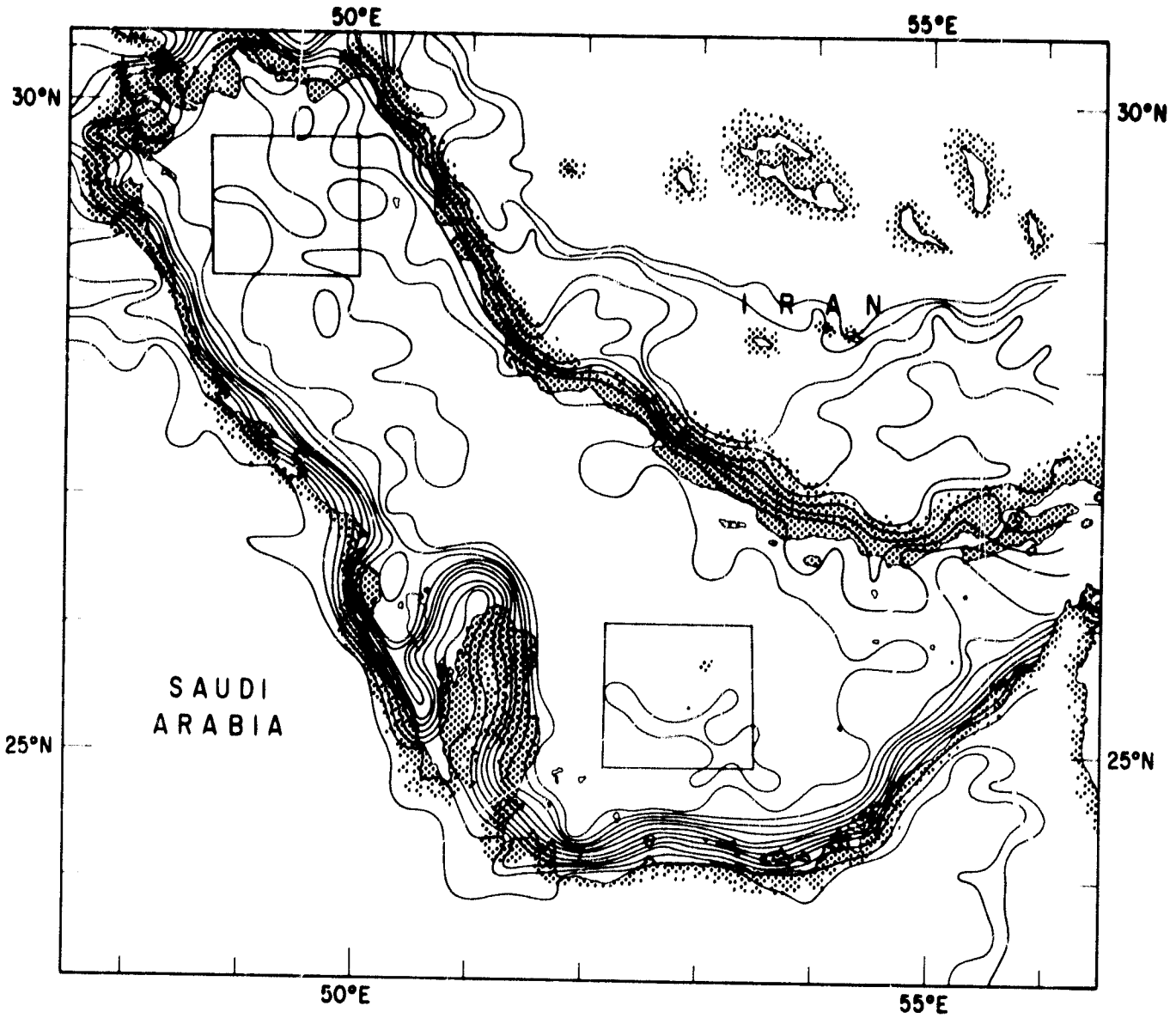

Fig. 2. Isolines and gradients obtained from Nimbus HRIR over the Persian Gulf on September 11, 1966. Included in this analysis is the coastline obtained from a nautical chart.

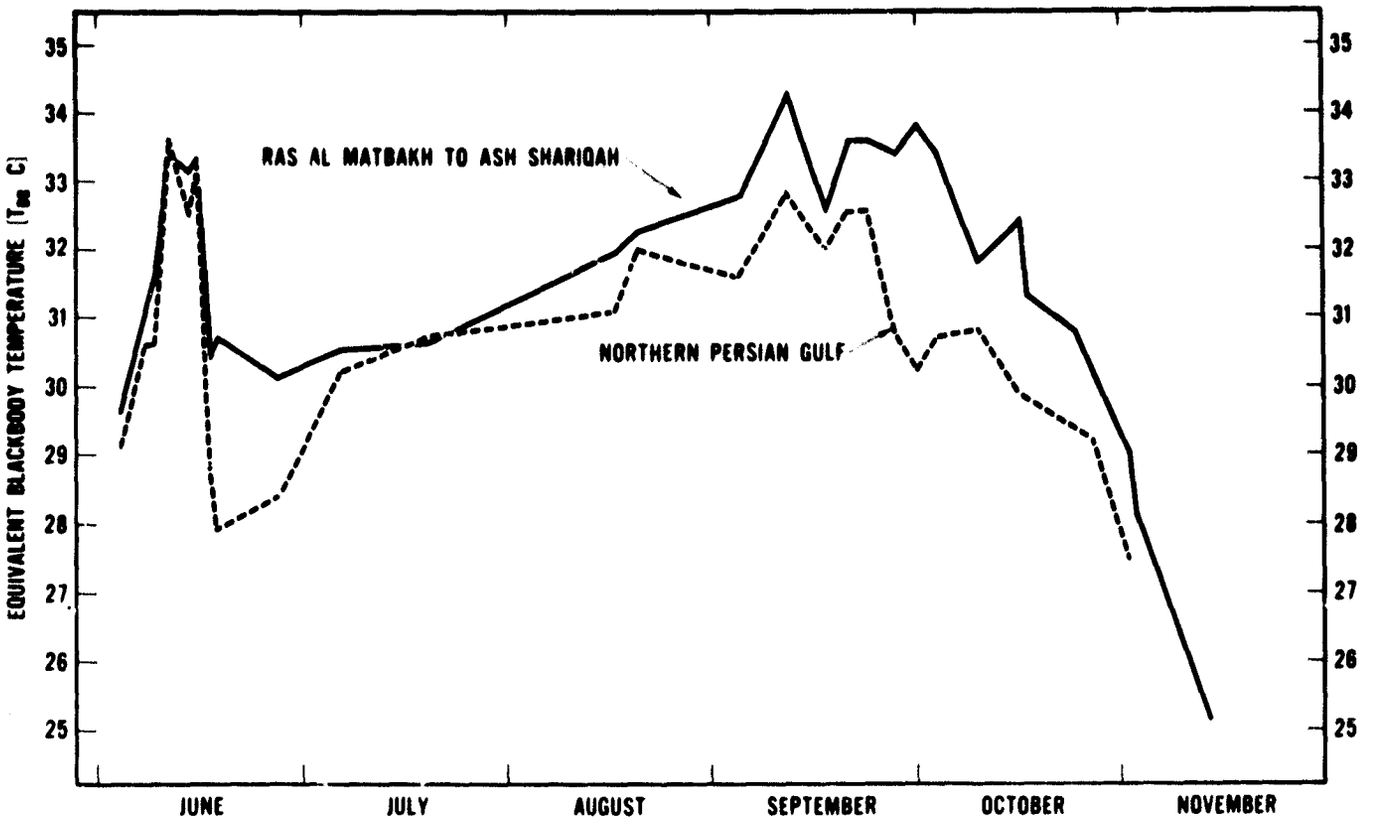

Fig. 3. Temperature fluctuations as derived from Nimbus 2 HRIR measurements over the Perisan Gulf in 1966. Dashed line shows the values for the northern region, and the solid line gives the temperature variation in the southern region.

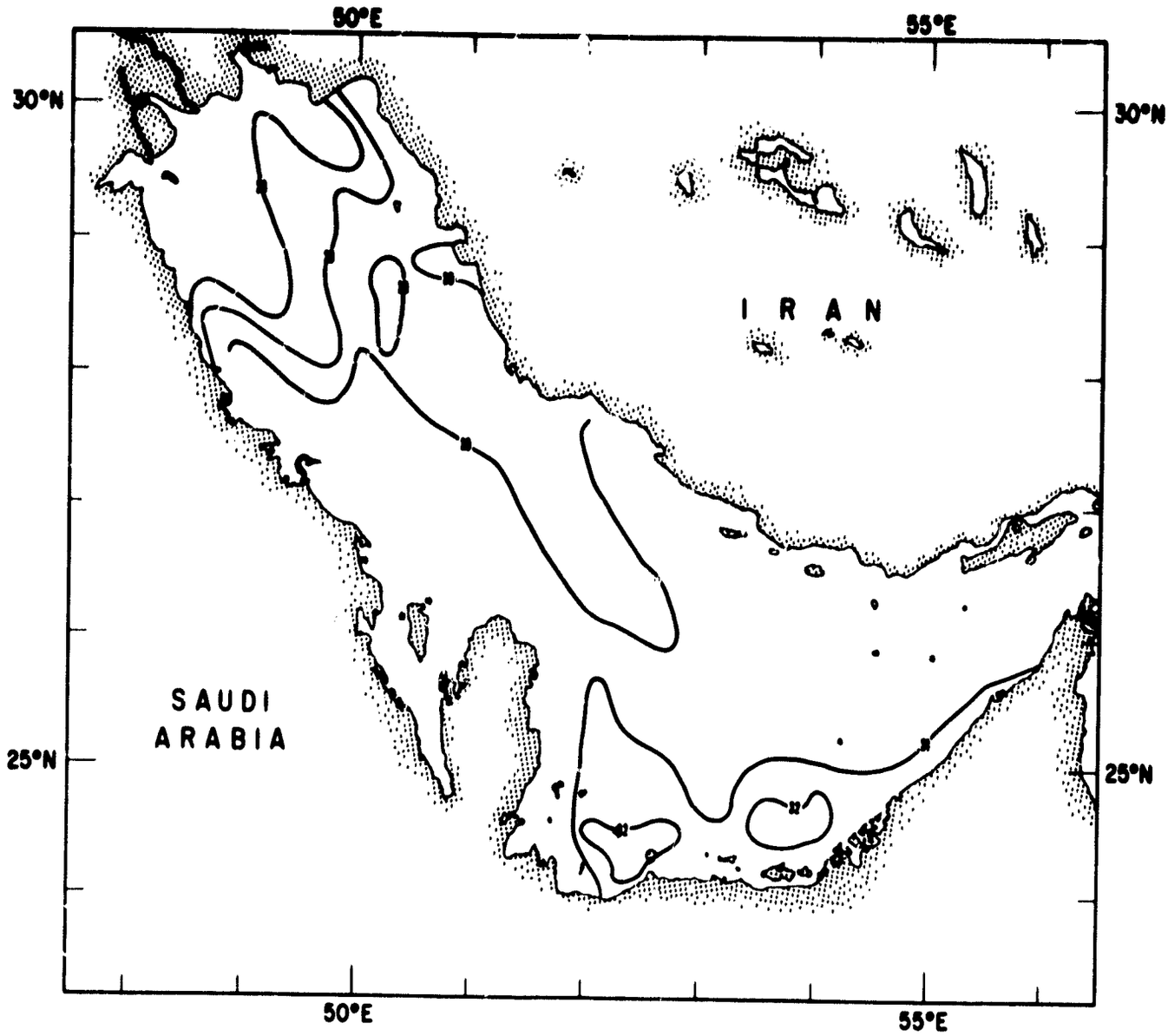

Fig. 4. Temperature distribution in the Persian Gulf on June 26, 1966.

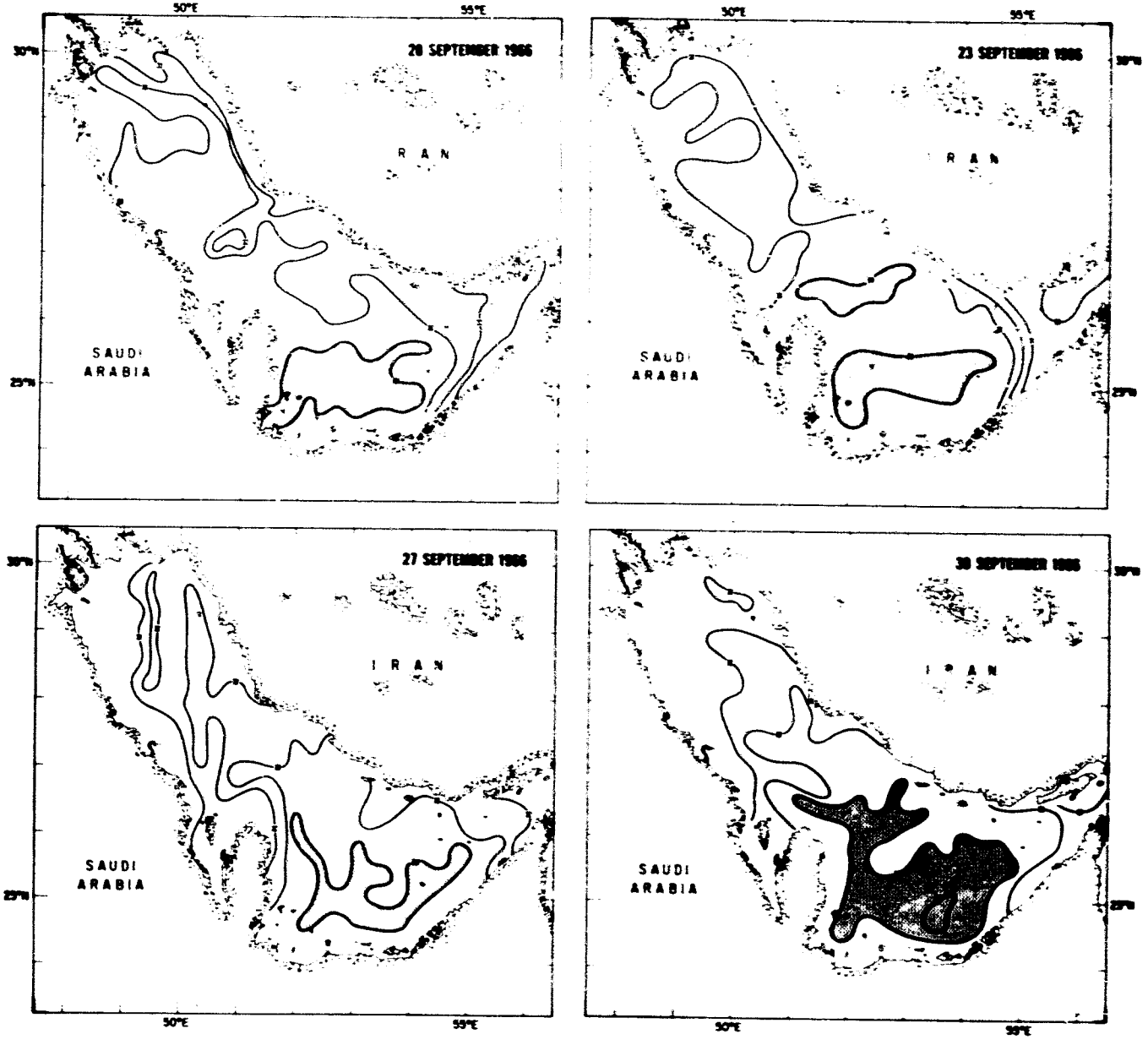

Fig. 5. Observations from nighttime orbits on September 20, 23, 27, and 30, 1966. Shaded areas show water temperatures above 34°C.

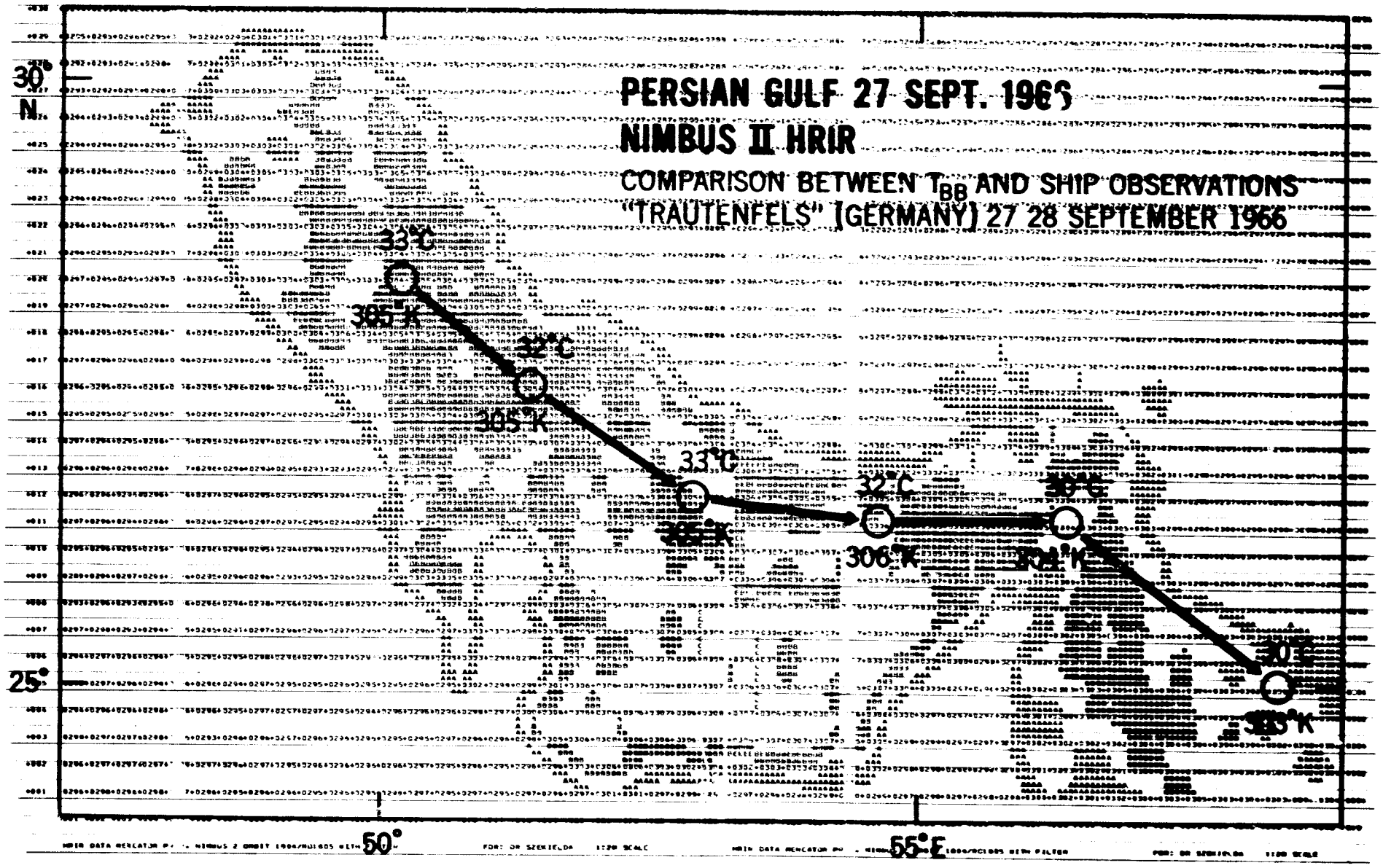

Fig. 6. Comparison between ship observations (Trautenfels) on September 27 and 28, 1966, and T_{BB} values from Nimbus 2 HRIR data obtained on September 27, 1966. The coastline is produced from a computer contouring program.

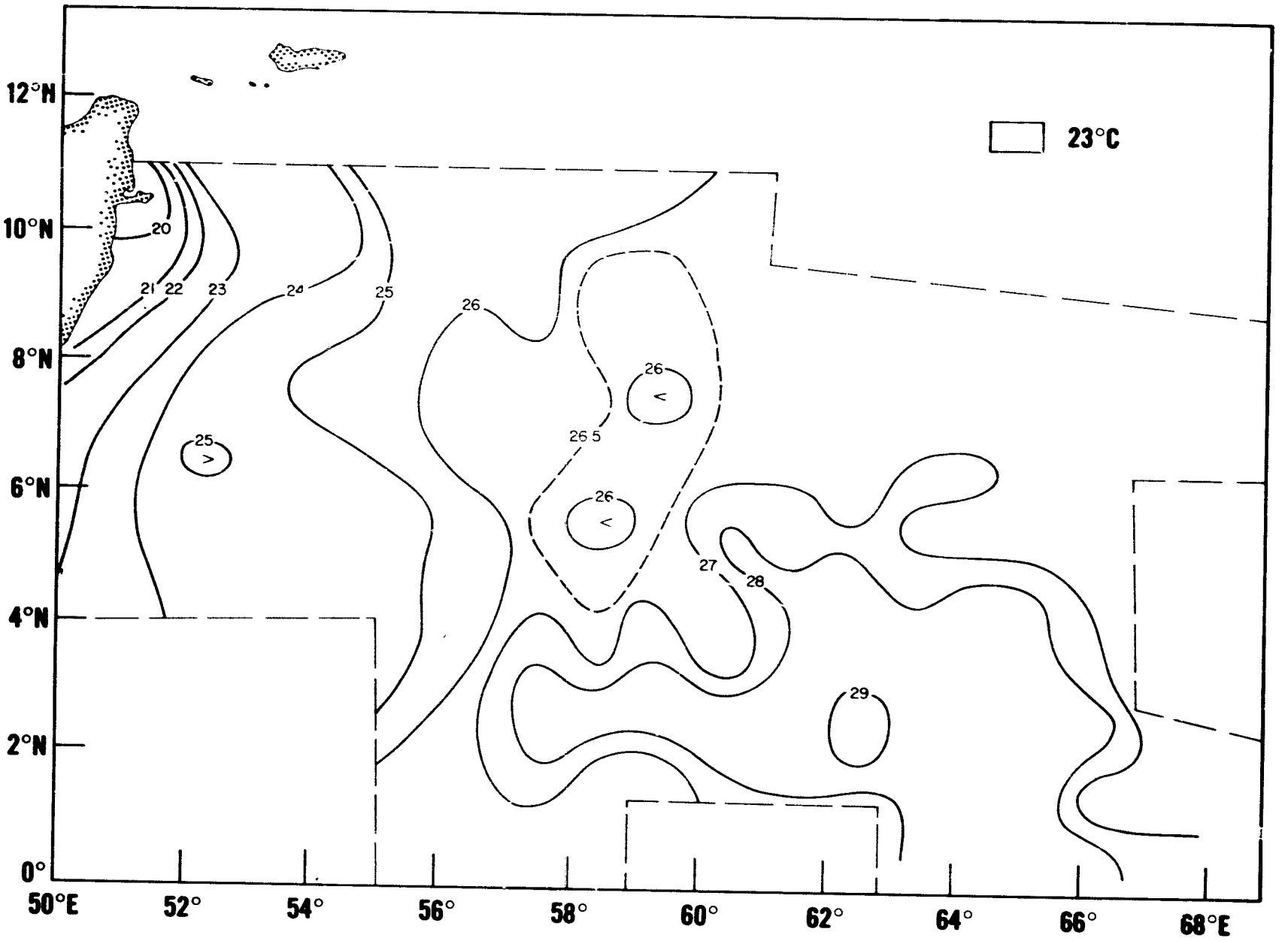

Fig. 7. T_{BB} distribution in the Arabian Sea on September 9, 1966, between 10°N and the equator.

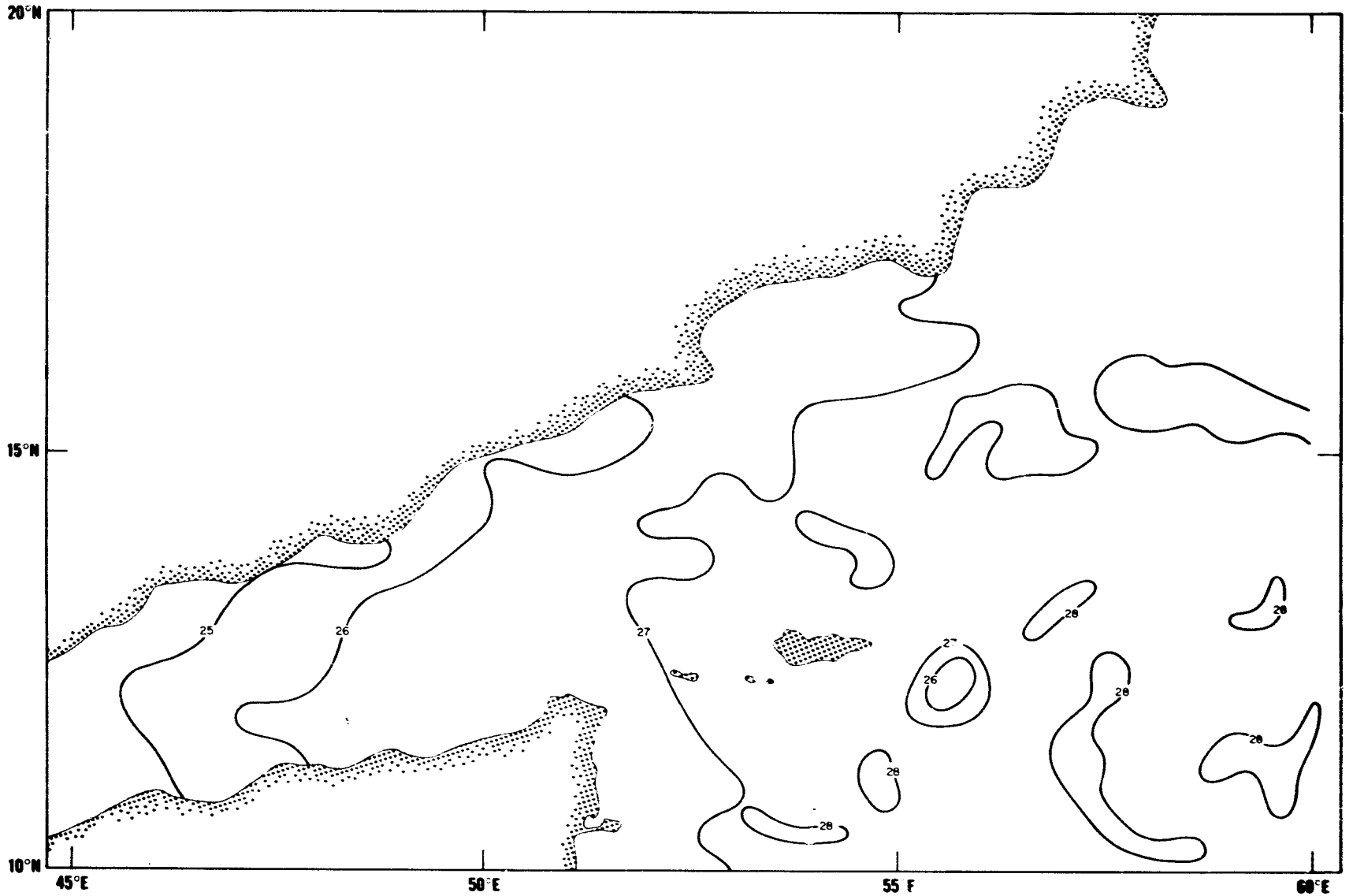

Fig. 8. T_{BB} distribution on May 23, 1966, in the northern Arabian Sea.

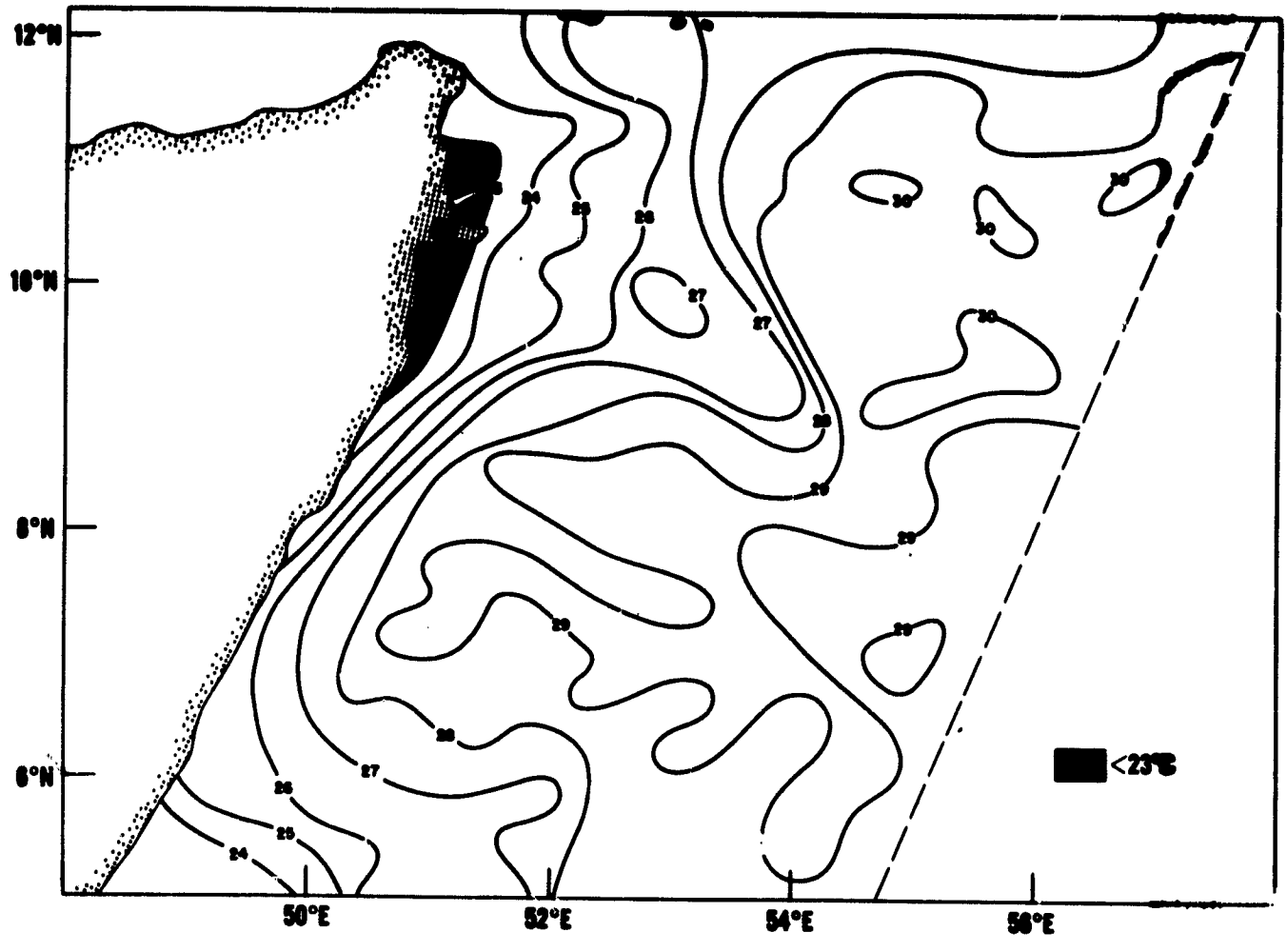

Fig. 9. T_{BB} distribution on June 8, 1966, along the Somali Coast.

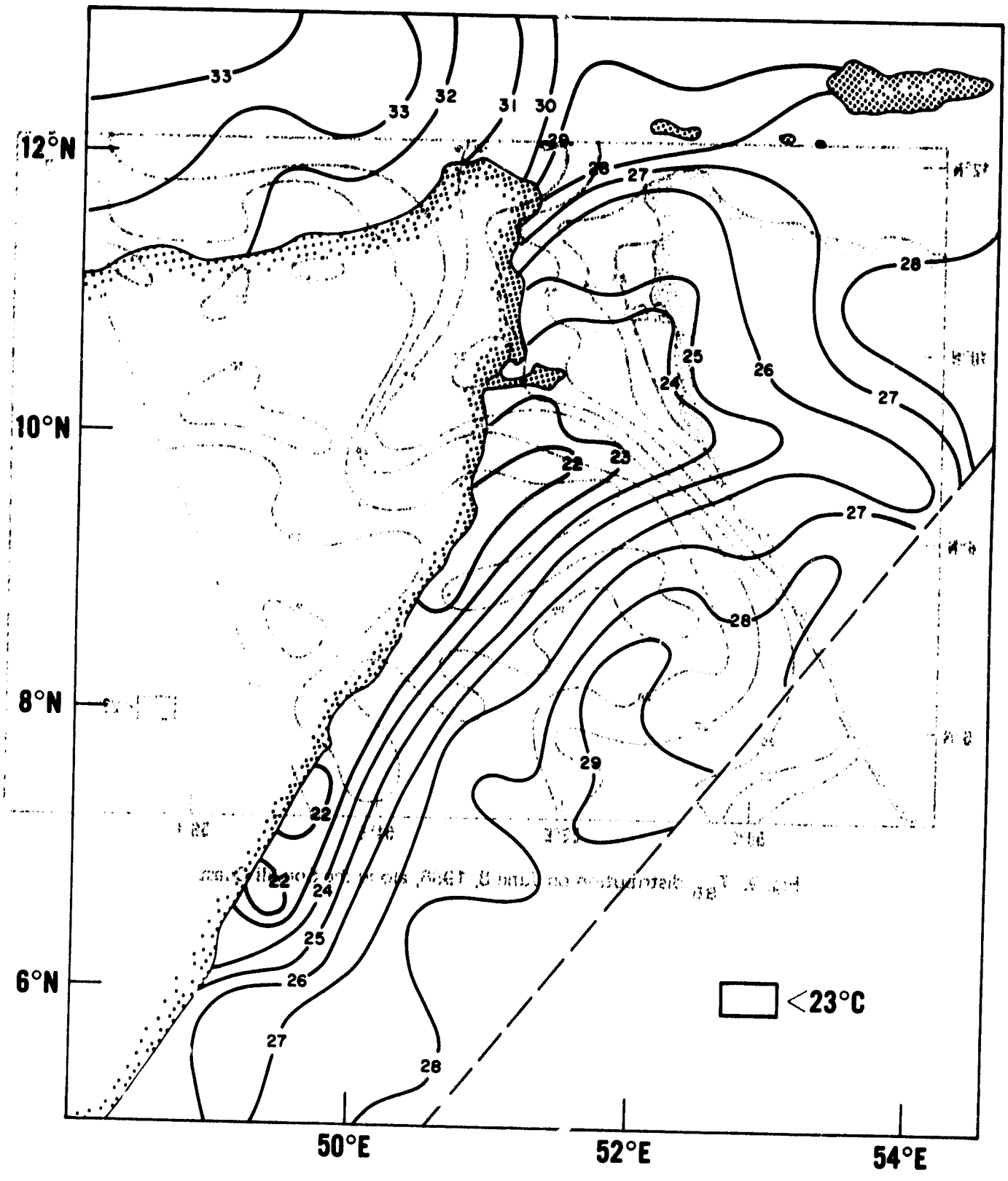

Fig. 10. T_{BB} distribution on June 10, 1966, along the Somali Coast.

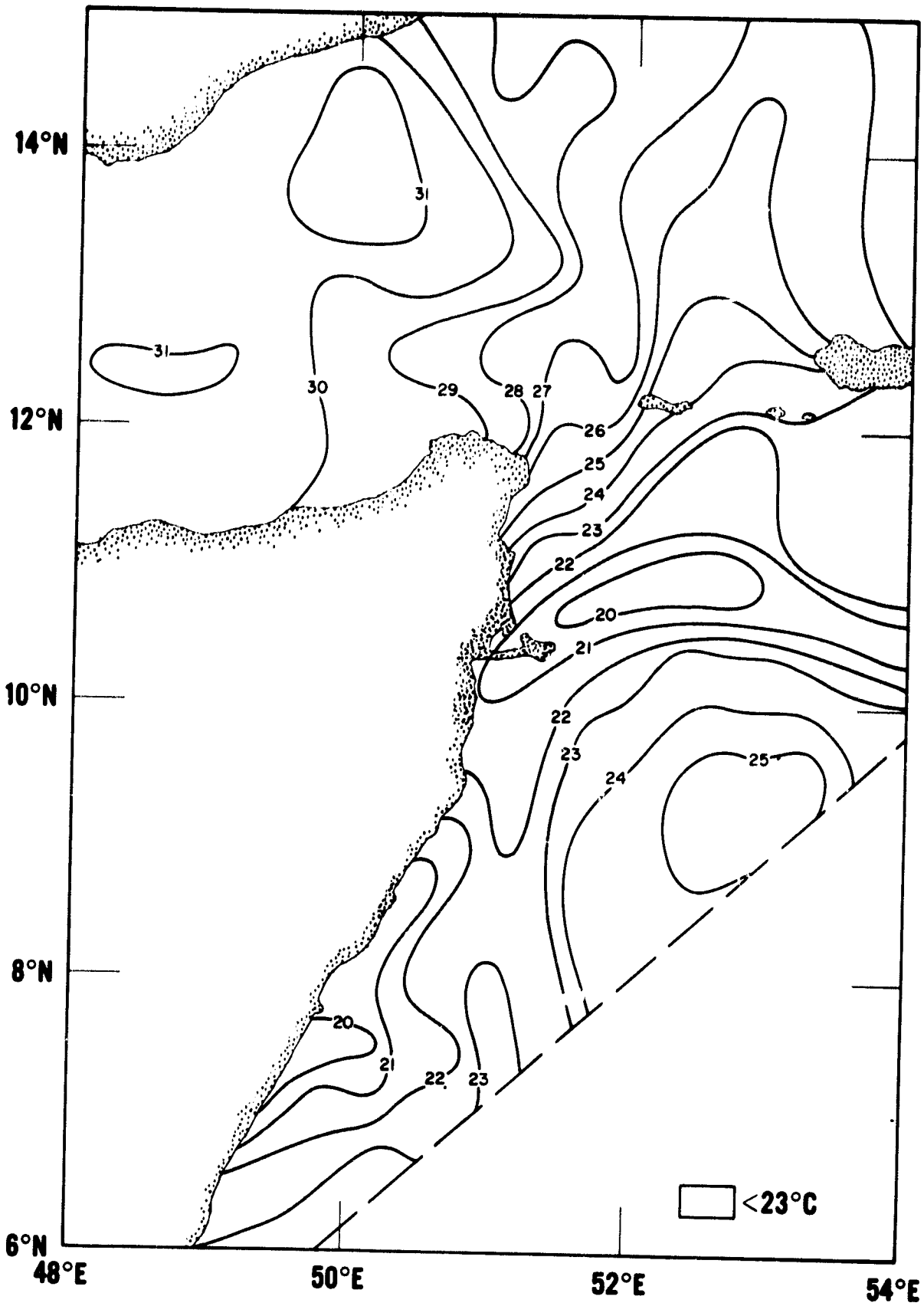

Fig. 11. T_{BB} distribution on July 2, 1966, along the Somali Coast.

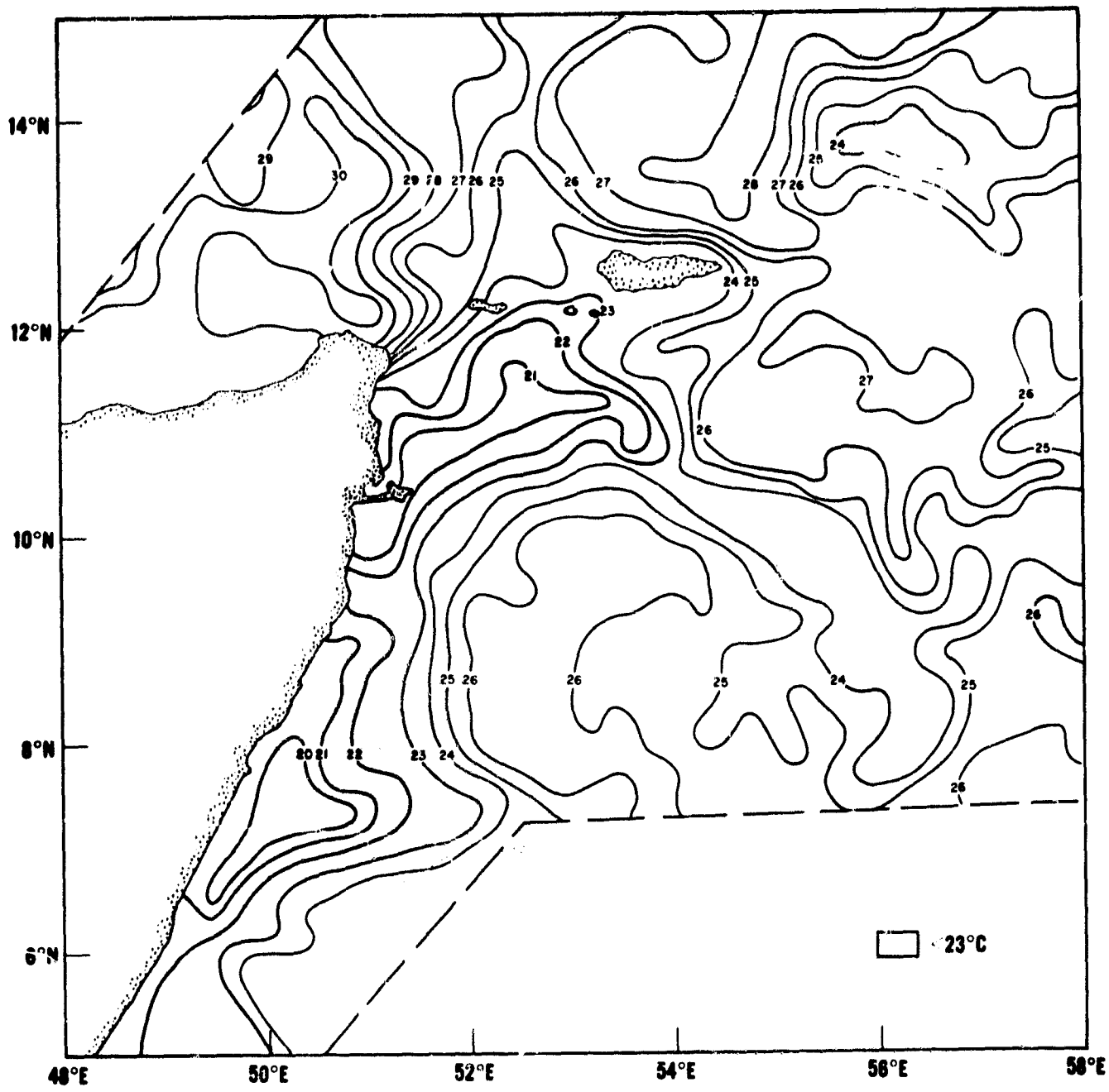

Fig. 12. T_{BB} distribution on July 3, 1966, along the Somali Coast (compare with Table 4).

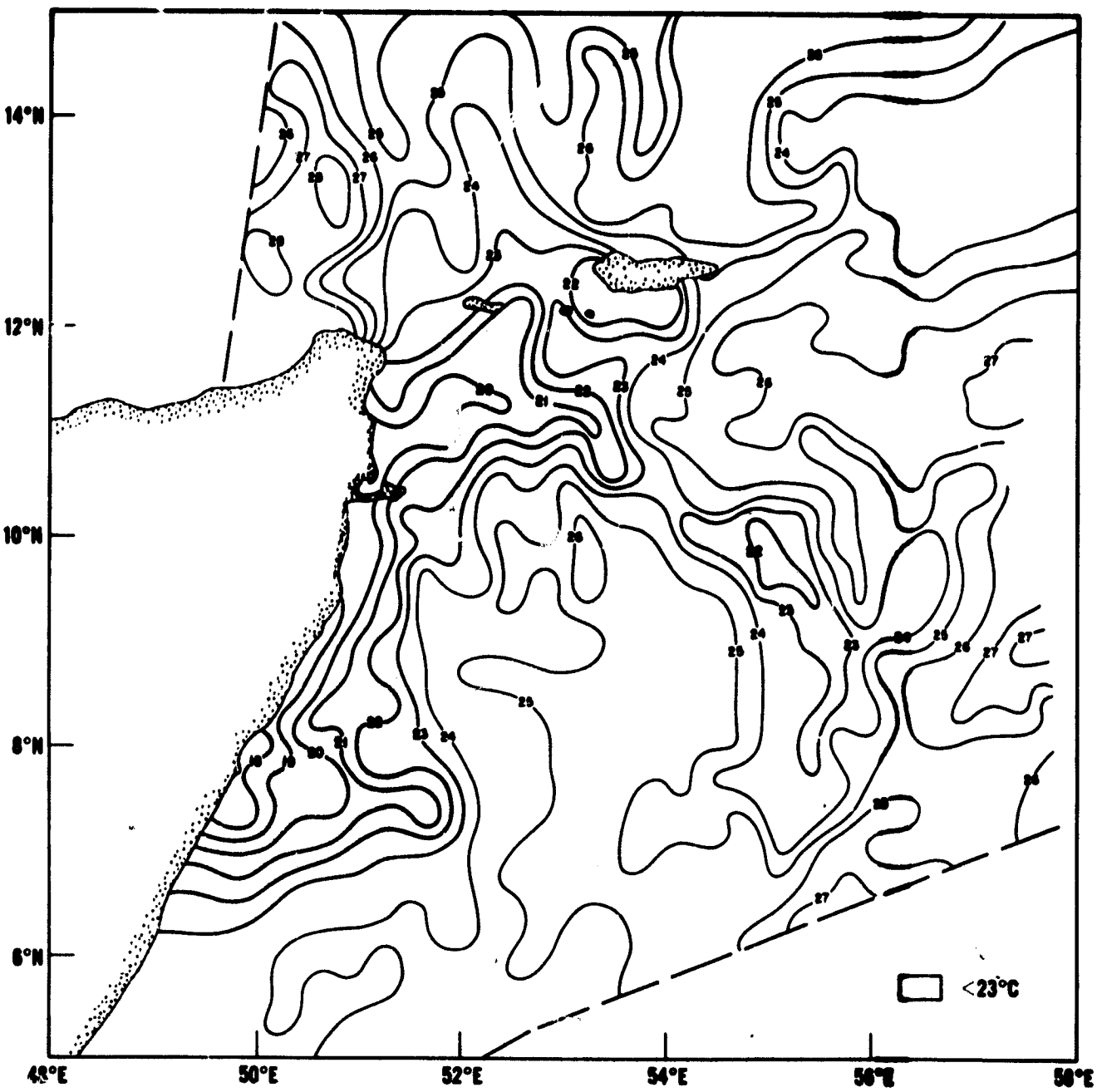

Fig. 13. T_{BB} distribution on July 4, 1966, along the Somali Coast (compare with Table 4).

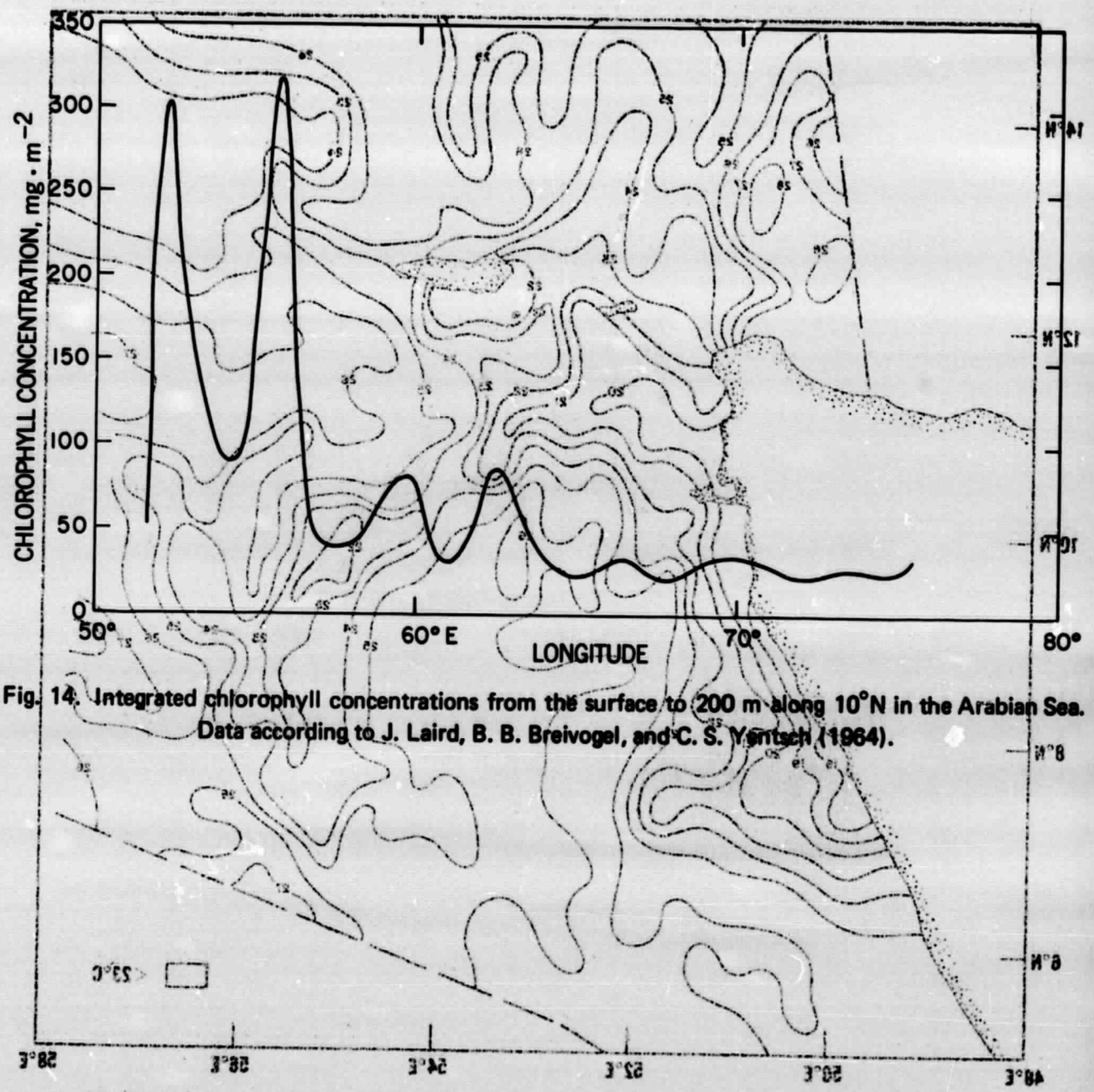

Fig. 14. Integrated chlorophyll concentrations from the surface to 200 m along 10°N in the Arabian Sea. Data according to J. Laird, B. B. Breivogel, and C. S. Yentsch (1964).

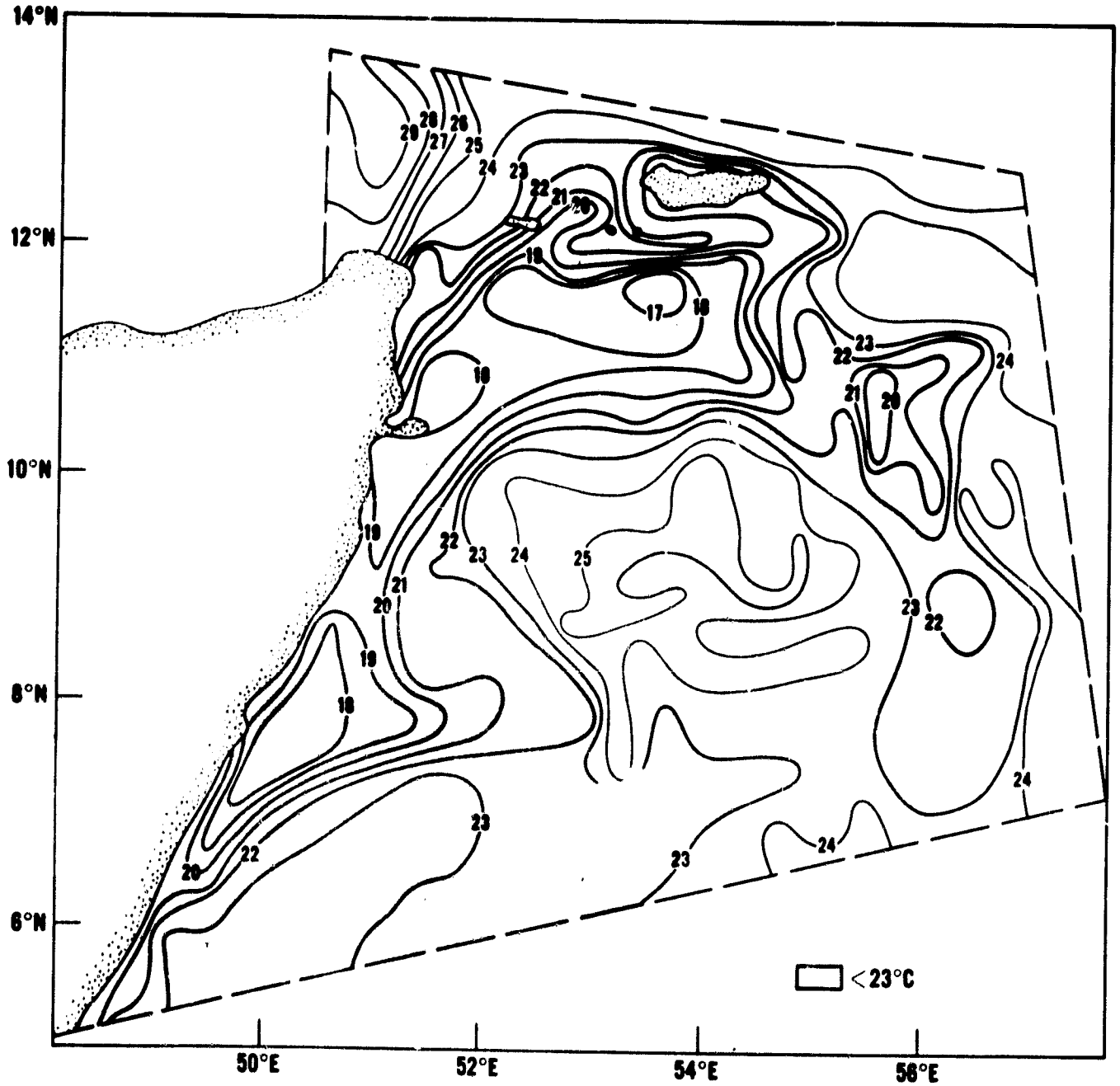

Fig. 15. T_{BB} distribution on July 6, 1966, along the Somali Coast.

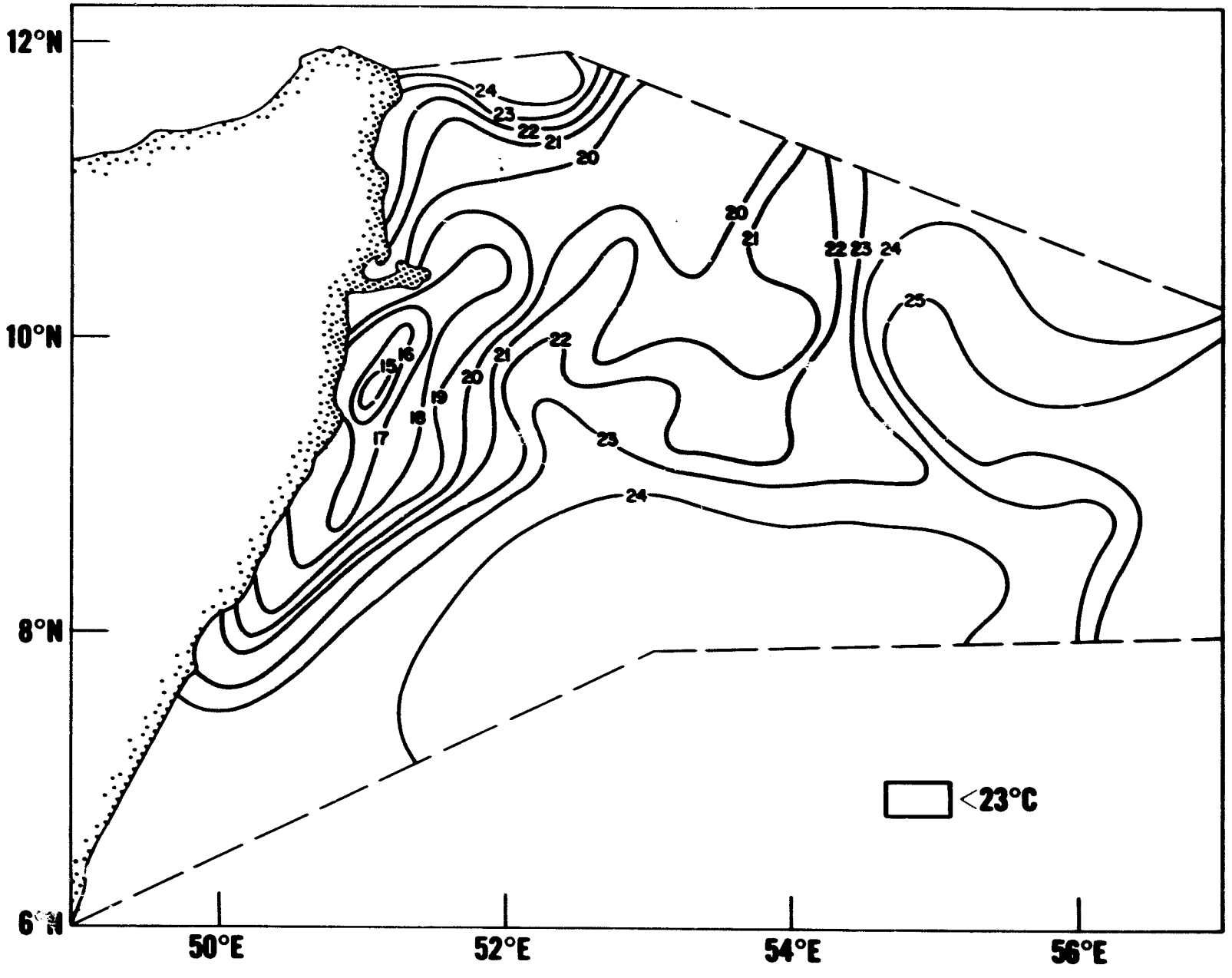

Fig. 16. T_{BB} distribution on July 16, 1966, along the Somali Coast.

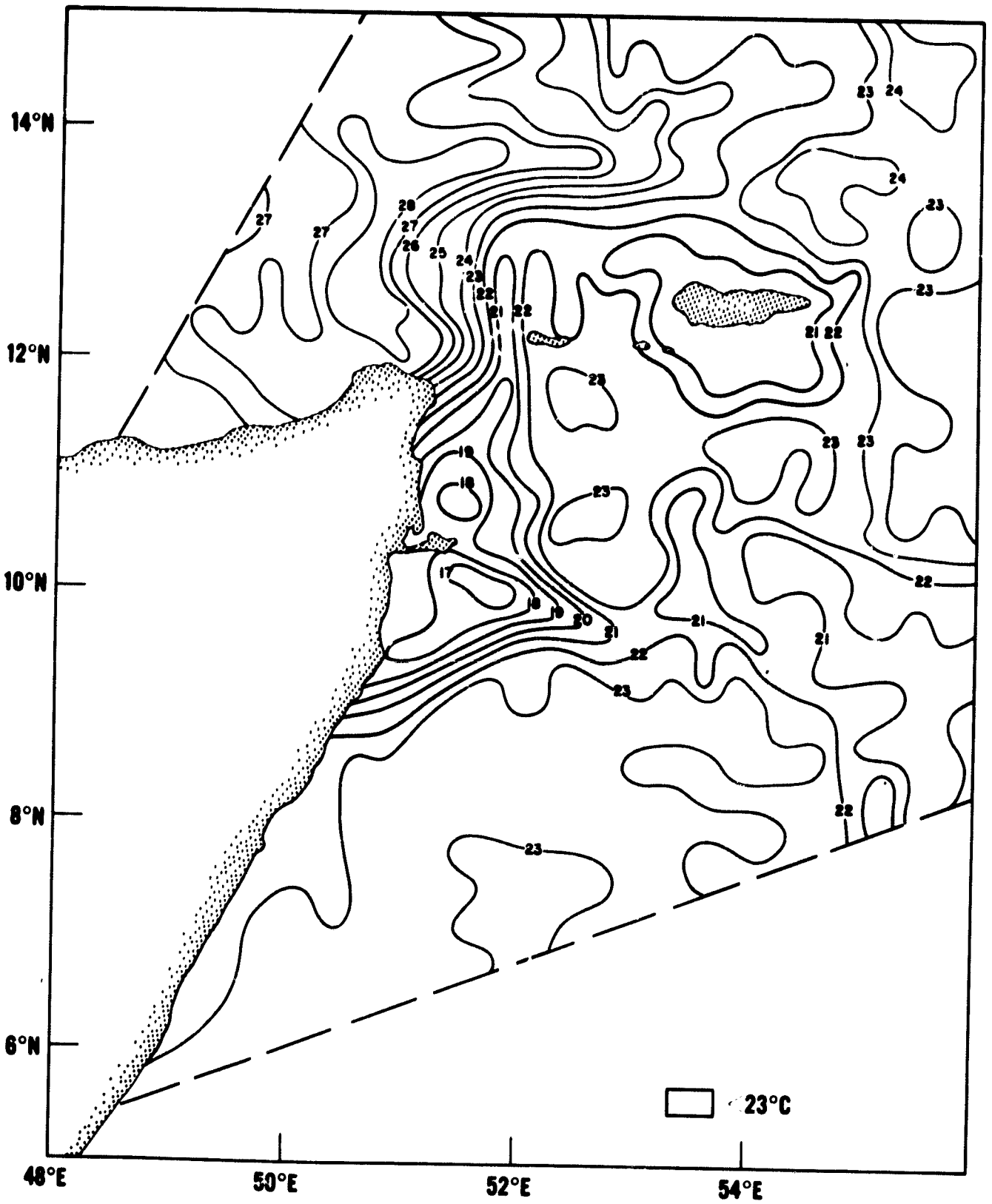

Fig. 17. T_{BB} distribution on August 13, 1966, along the Somali Coast.

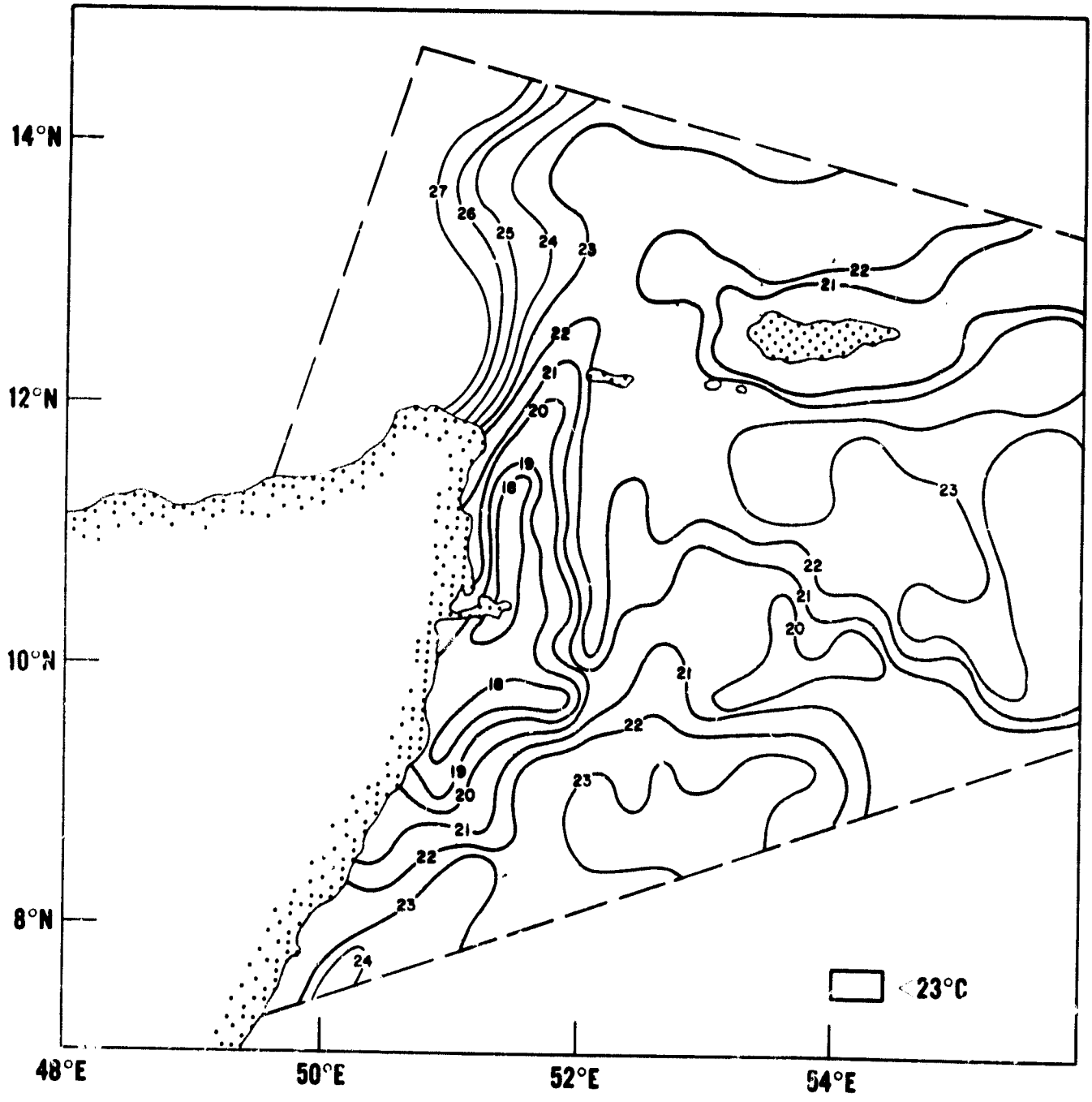

Fig. 18. T_{BB} distribution on August 16, 1966, along the Somali Coast.

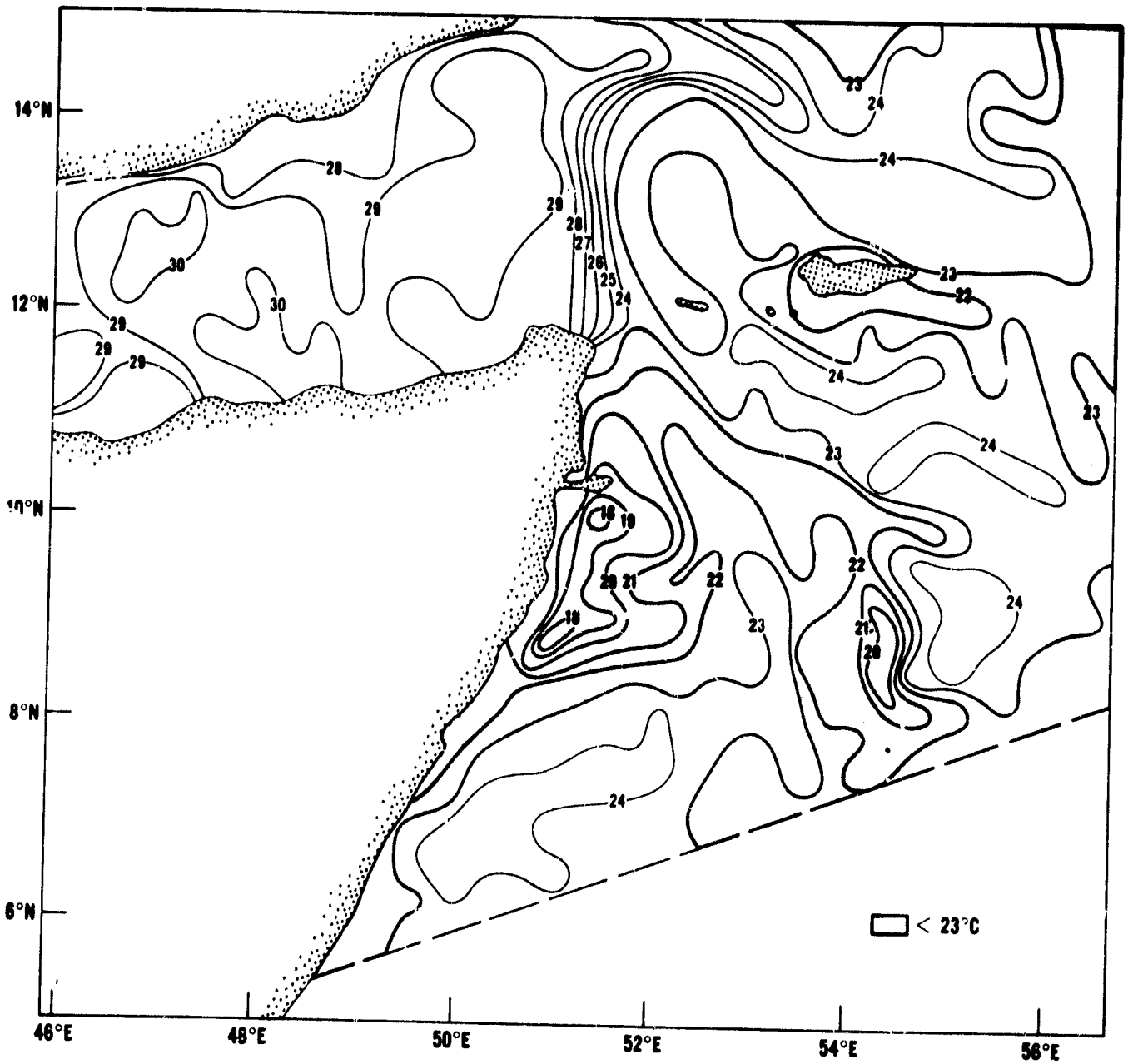

Fig. 19. T_{BB} distribution on September 4, 1966, along the Somali Coast.

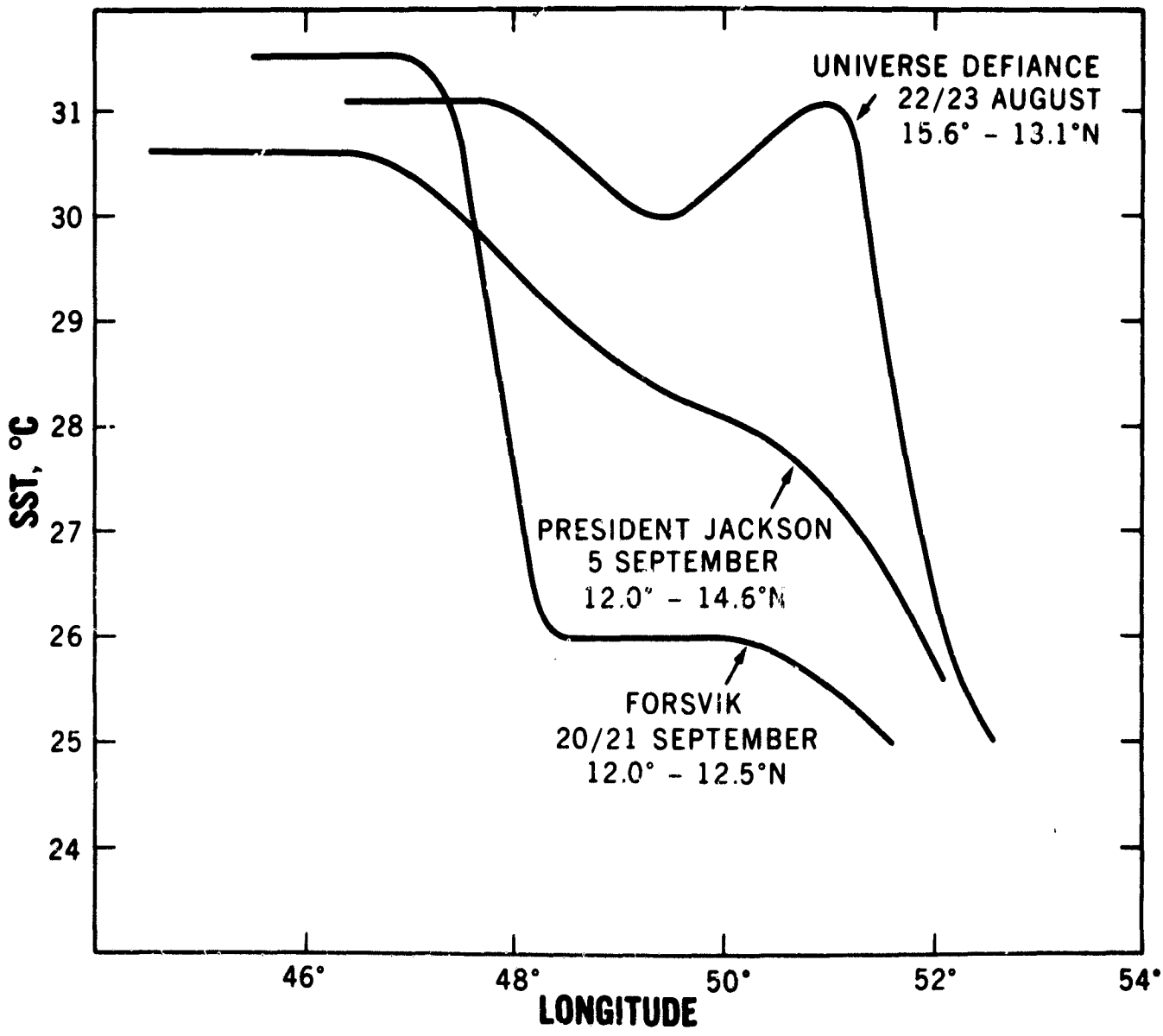

Fig. 20. Selected examples of conventional ship observations of SST in the Gulf of Aden and the adjacent sea in August and September 1966.

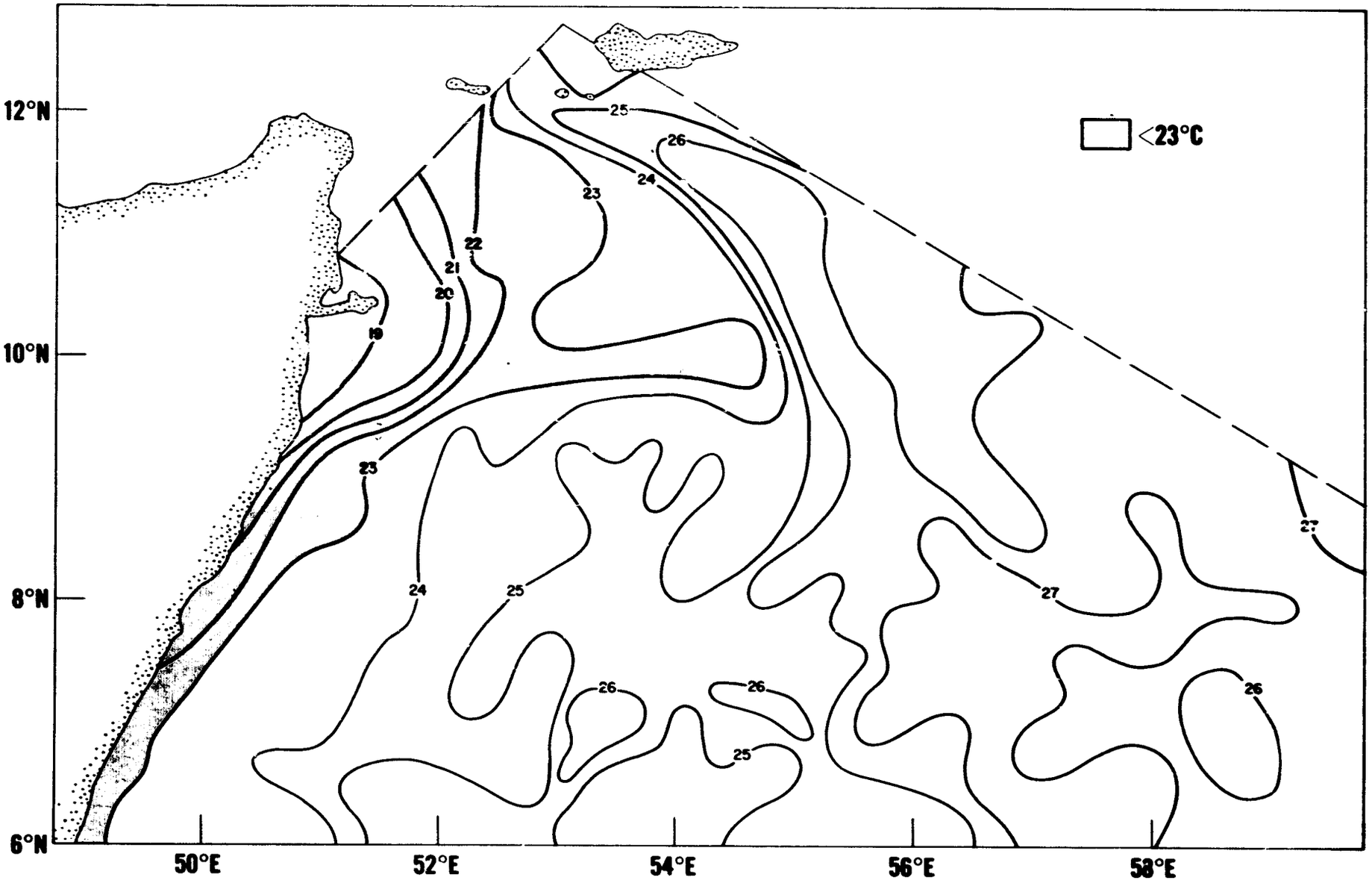

Fig. 21. T_{BB} distribution on September 9, 1966, along the Somali Coast.

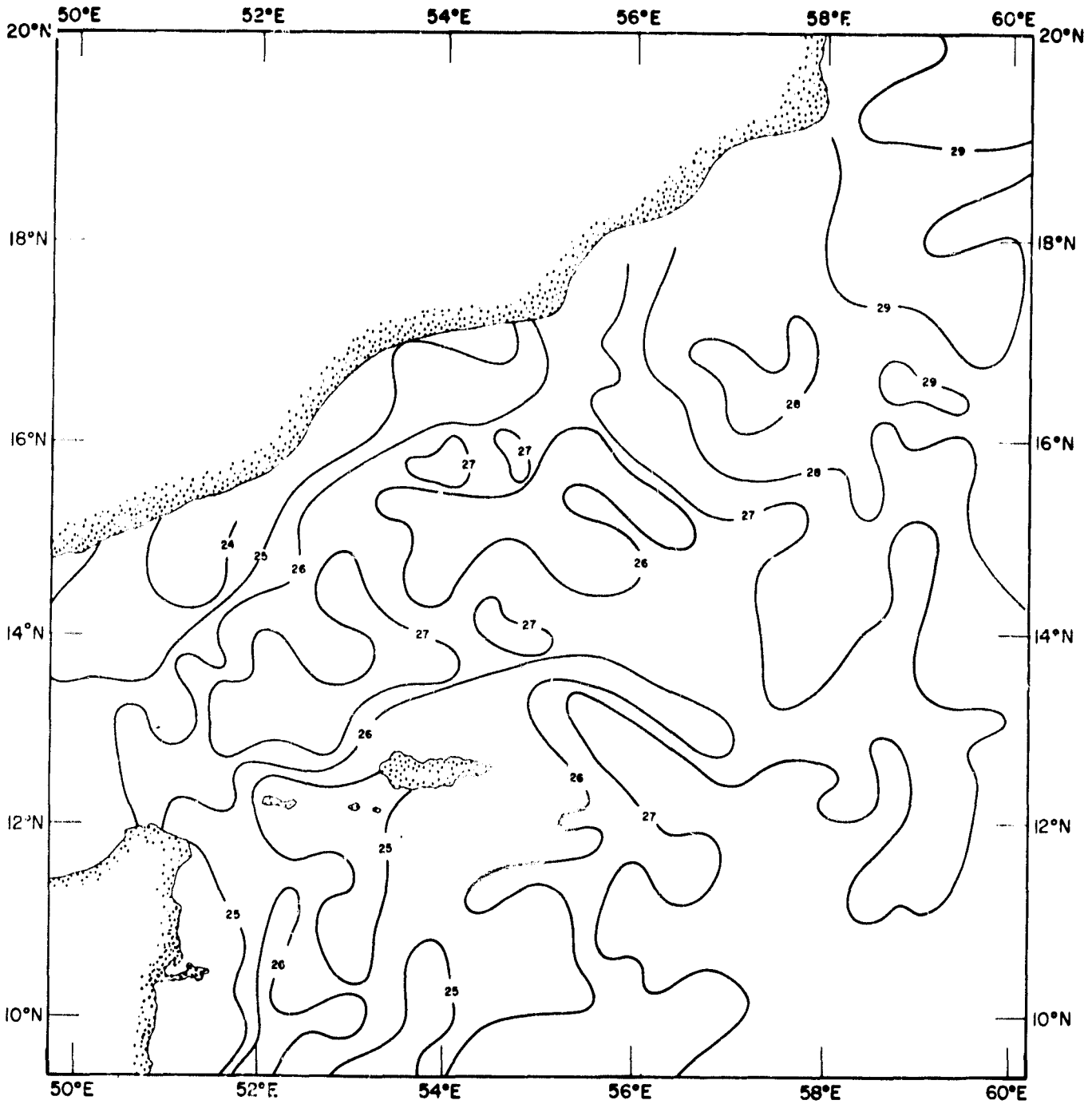

Fig. 22. T_{BB} distribution along the Somali Coast and a portion of the northern Arabian Sea on October 30, 1966.

Fig. 23. Negative print from an Apollo 7 color photograph taken in October 1967 between Socotra and the Somali Coast. The gyre has a diameter of about 50 kilometers.

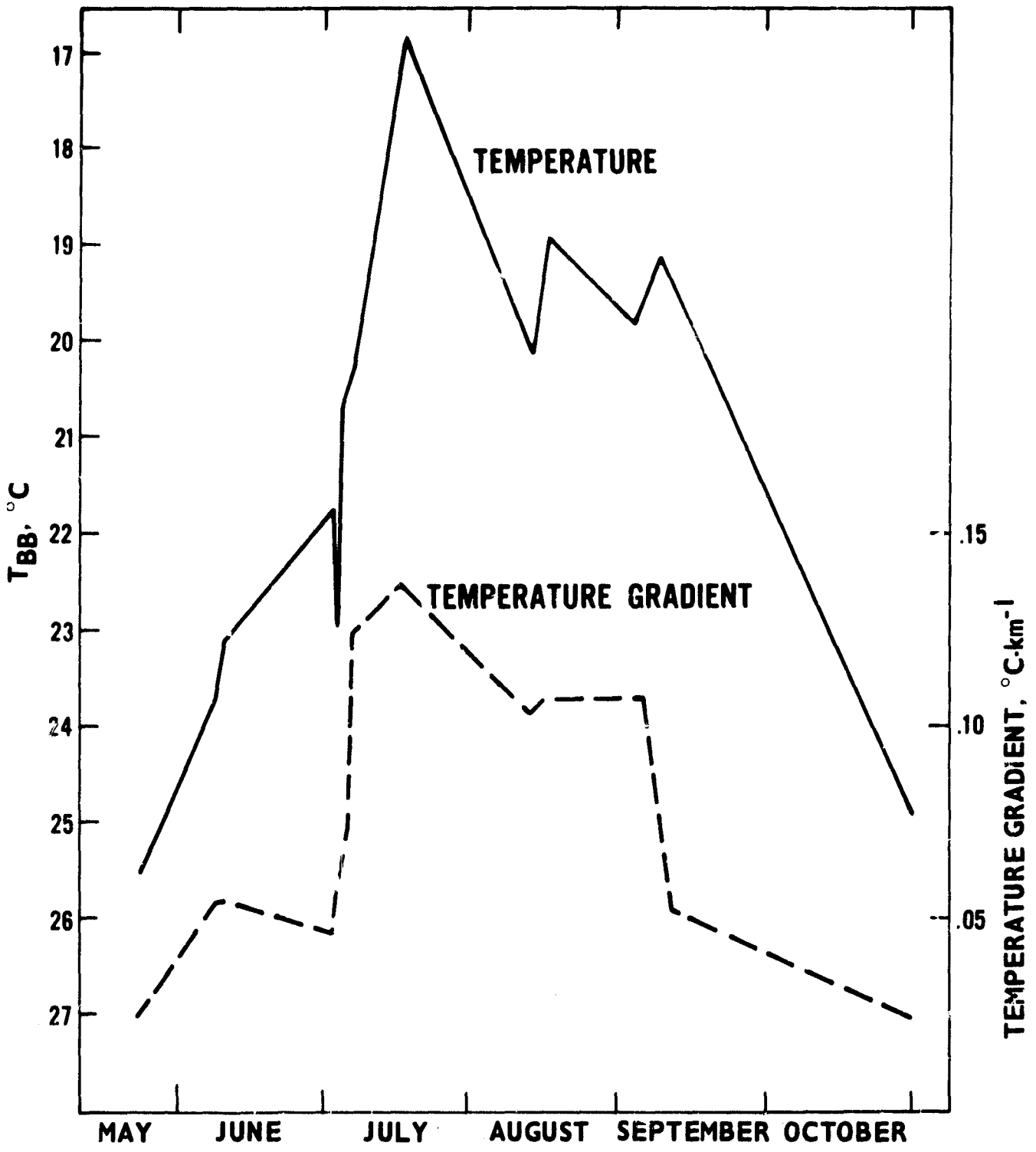

Fig. 24. T_{BB} change in the center of the upwelling along the Somali Coast. Mean values are built from 8° to 10°N between the coast and 52°E.

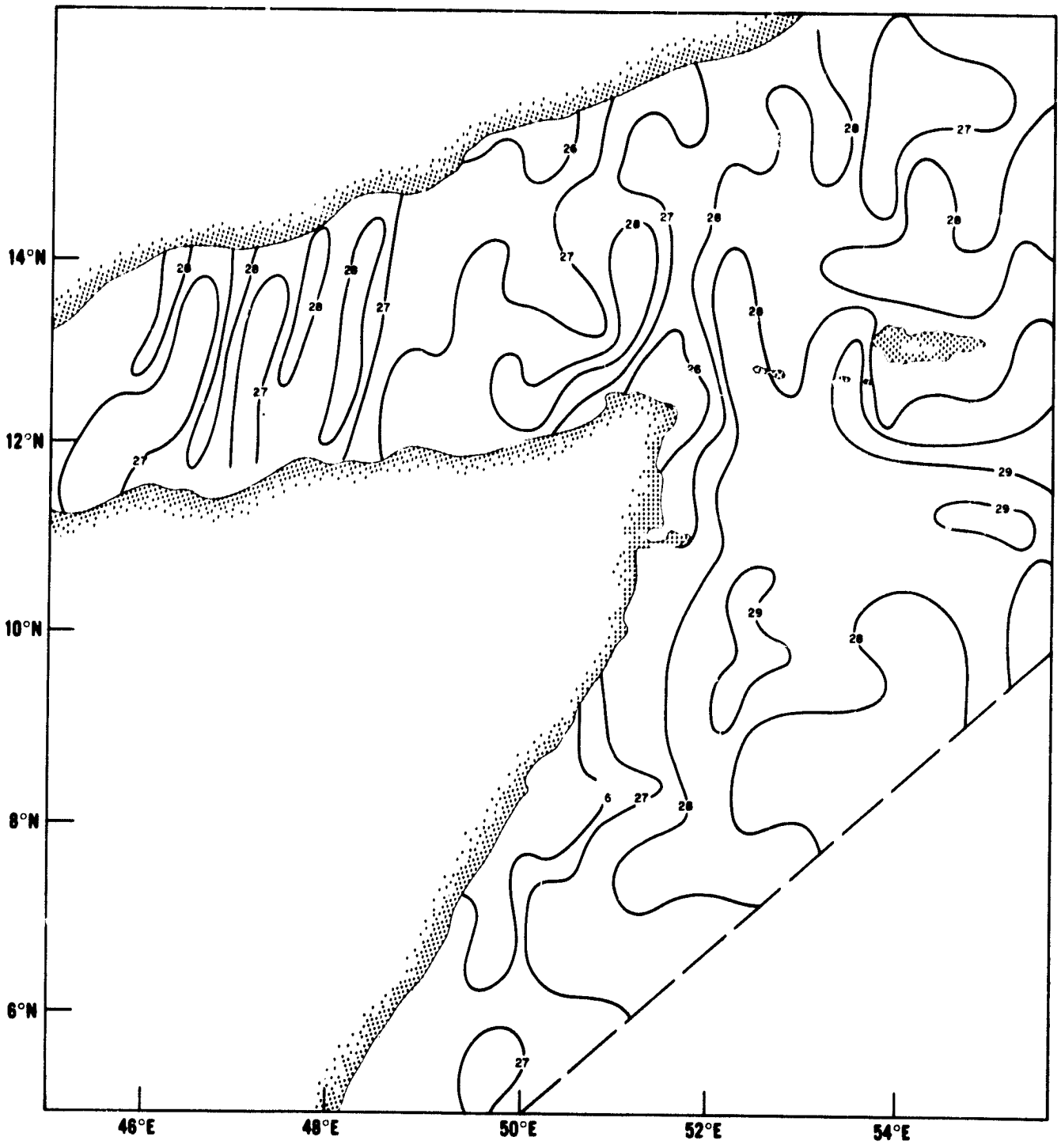

Fig. 25. T_{BB} distribution on May 14, 1969, along the Somali Coast.

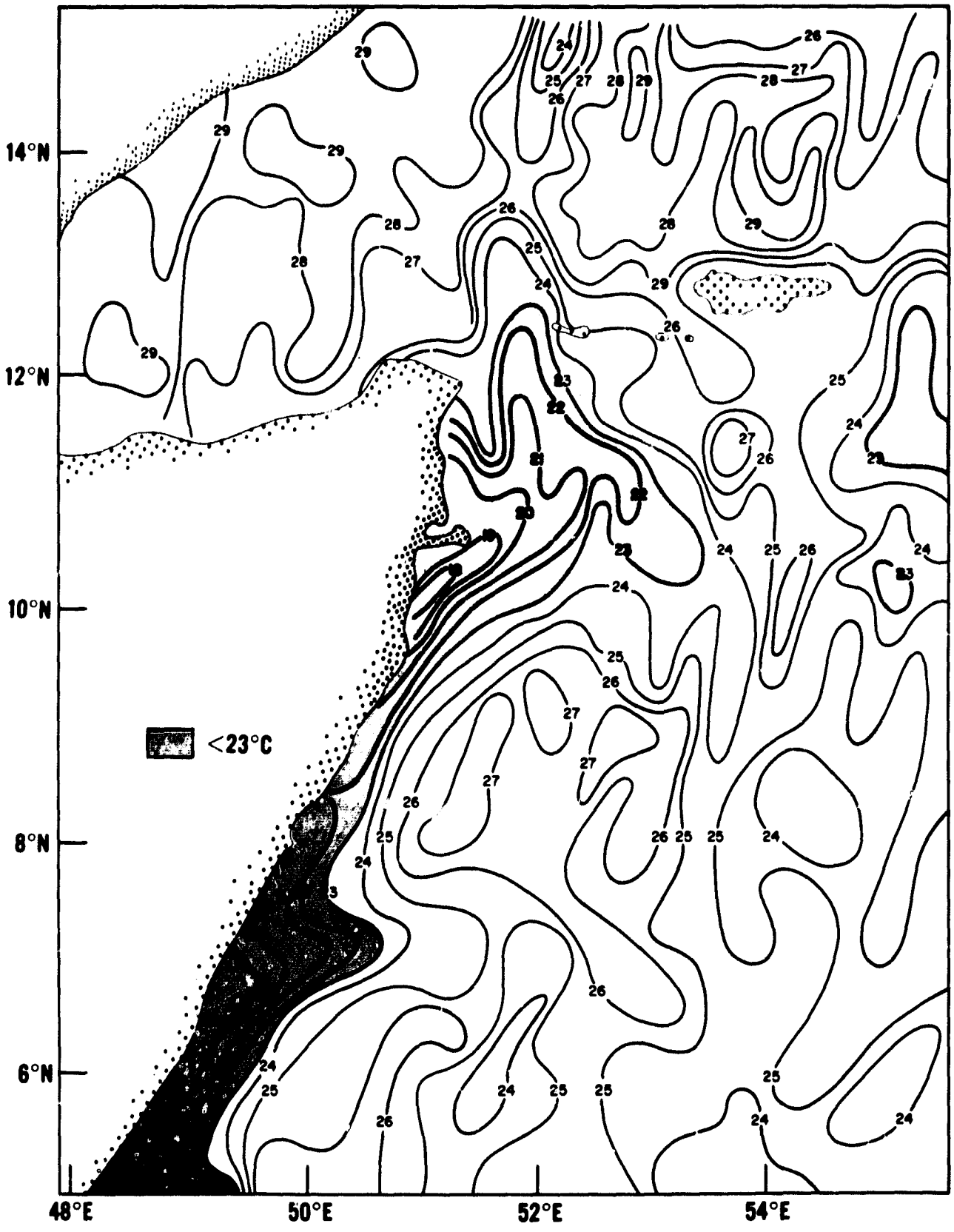

Fig. 26. T_{BB} distribution on May 31, 1969, along the Somali Coast.